

6.09 High-Valent Ni Coordination Compounds

Neil Heberer*, Chi-Herng Hu*, and Liviu M. Mirica, Department of Chemistry, University of Illinois at Urbana-Champaign, Urbana, IL, United States

© 2021 Elsevier Ltd. All rights reserved.

6.09.1	Introduction	349
6.09.2	Ni(III) and Ni(IV) Complexes	349
6.09.2.1	Complexes Stabilized With All-Nitrogen Ligands	349
6.09.2.1.1	Ni-imide complexes	349
6.09.2.1.2	Ni-oxo and Ni-peroxo complexes	349
6.09.2.1.3	Ni-cyclam complexes	351
6.09.2.1.4	Ni complexes with silyl-anilide ligands	351
6.09.2.1.5	Ni complexes with macrocyclic N4 ligands	351
6.09.2.1.6	Dinuclear Ni complexes	352
6.09.2.2	Ni Complexes With All-Carbon Ligands	353
6.09.2.2.1	Ni complexes with all-alkyl ligands	353
6.09.2.2.2	Ni complexes with NHC-type ligands	354
6.09.2.3	Ni Complexes With Mixed Nitrogen-Oxygen Ligands	354
6.09.2.3.1	Ni complexes with Schiff base ligands	354
6.09.2.3.2	Ni complexes with pyridine-alkoxide ligands	354
6.09.2.4	Ni Complexes With Mixed Nitrogen-Sulfur Ligands	355
6.09.2.4.1	Ni complexes with imine-thiolate ligands	355
6.09.2.4.2	Ni complexes with aza-thioether ligands	356
6.09.2.5	Ni Complexes With Mixed Phosphorus-Sulfur Ligands	356
6.09.2.5.1	Ni complexes with tris(thiolate)-phosphine ligands	356
6.09.2.5.2	Ni complexes with mixed phosphorus-thiolate ligands	358
6.09.2.6	Ni Complexes With Mixed Nitrogen-Carbon Ligands	360
6.09.2.6.1	Ni complexes with tris(2-pyridylthio)methanide ligands	360
6.09.2.6.2	Ni complexes with macrocyclic N ₃ C ligands	360
6.09.2.6.3	Ni complexes with pyridine-aromatic amine ligands	360
6.09.2.6.4	Ni complexes with tris(pyrazolyl)borate ligands	362
6.09.2.7	Ni Complexes With Pincer Ligands	362
6.09.2.7.1	Ni complexes with POCOP pincer ligands	362
6.09.2.7.2	Ni complexes with POCN pincer ligands	363
6.09.2.7.3	Ni complexes with PCN pincer ligands	364
6.09.2.7.4	Ni complexes with NCN pincer ligands	364
6.09.2.7.5	Ni complexes with NHC pincer ligands	365
6.09.2.8	Ni Complexes With Perfluoroalkyl Ligands	365
6.09.2.9	Ni Complexes With Cycloneophyl Ligands	367
6.09.2.10	Ni Complexes With Miscellaneous Ligands	370
6.09.3	Summary and Outlook	373
References		373

Key Terms

High-valent Ni(III) and Ni(IV) complexes These have seen a burgeoning of interest over the last two decades. This can be attributed to the presence of Ni(III) in some bioinorganic enzyme active sites along with the demonstrated role of Ni(III) and Ni(IV) in carbon-carbon and carbon-heteroatom bond forming reactions.

Organometallic high-valent Ni complexes The field of organometallic nickel chemistry has grown extensively, as specifically tailored ligands have been designed that can be used to stabilize uncommon high-valent organometallic complexes.

*These authors contributed equally.

6.09.1 Introduction

The chemistry of high-valent Ni(III) and Ni(IV) complexes has seen a burgeoning of interest over the last two decades. This can be attributed to the presence of Ni(III) in some bioinorganic enzyme active sites along with the demonstrated role of Ni(III) and Ni(IV) in carbon-carbon and carbon-heteroatom bond forming reactions.^{1,2} Furthermore, the field of organometallic nickel chemistry has grown extensively, as specifically tailored ligands have been designed that can be used to stabilize uncommon high-valent organometallic complexes.³⁻⁵

Nickel centers in the +3 oxidation state adopt a d^7 electron configuration and prefer five-coordinate square pyramidal and trigonal bipyramidal geometries, or six-coordinate octahedral complexes that are Jahn-Teller distorted. In the +4 oxidation state, nickel has a d^6 electron configuration and is found almost exclusively in an octahedral geometry.^{6,7} Rare examples of four-coordinate Ni(IV) complexes which adopt distorted tetrahedral geometries have been observed, although they require extremely bulky ligands for stabilization.⁸ In both its +3 and +4 oxidation state, strong σ and π -donor ligands are required to stabilize the highly oxidized Ni center.

A wide variety of ligand frameworks have been successfully utilized to stabilize Ni(III) and Ni(IV) complexes over the last 20 years, and for the purposes of this review they have organized complexes based on the type of donor atoms, as well as special organic ligands that have been particularly useful for limiting the further reactivity of the isolated high-valent Ni complexes. Moreover, herein we have described the Ni(III) and Ni(IV) complexes that have been reported after 2003 and have been crystallographically characterized. To keep this chapter concise, we have not included the many reported examples of bis-dithiolene Ni complexes, in which the oxidation state of the metal center is sometimes not unambiguously known,⁹⁻¹³ or the examples of oxidized coordination polymers or 1-D Chains in which the Ni centers can be found in mixed-valent states.¹⁴⁻¹⁷

6.09.2 Ni(III) and Ni(IV) Complexes

6.09.2.1 Complexes Stabilized With All-Nitrogen Ligands

6.09.2.1.1 Ni-imide complexes

Metal imide complexes have been demonstrated to be intermediates in alkene aziridination and other C–N bond forming reactions, and in 2005 Warren et al. isolated a three-coordinate Ni(III)-imido complex **1** (Fig. 1).¹⁸ EPR studies of **1** at 77 K indicated a rhombic geometry ($g_1 = 2.162$, $g_2 = 2.038$, and $g_3 = 1.937$), with the $g = 2.038$ signal showing as a 1:1:1 triplet with a superhyperfine coupling constant of $A = 22$ G. The presence of this signal suggested there is significant interaction of the imido nitrogen with the singly occupied d_{xy} orbital of this low-spin Ni(III) complex, and this was verified through DFT calculations, which revealed appreciable spin density on the imido nitrogen due to the two-center three-electron interaction between the Ni d_{xy} orbital and the imido N p_x orbital.

6.09.2.1.2 Ni-oxo and Ni-peroxo complexes

The tetradentate ligand Me₃tpa was used by Suzuki et al. to isolate the Ni(III)-Ni(III) μ -oxo dinuclear complex **2** in 2006 (Fig. 2).¹⁹ X-ray crystallography of **2** showed a centrosymmetric Ni^{III}(μ -O)₂Ni^{III} core with average Ni–O bond lengths of 1.852 Å and a Ni–Ni distance of 2.796 Å, and large variations in the Ni–N bond distances based on the equatorial vs. the axial positions (1.975 Å vs. 2.285 Å, respectively) were also observed. The elongation of the axial Ni–N bonds was attributed to Jahn-Teller distortion arising from the low-spin d^7 electronic configuration. A similar bis(μ -oxo)dinickel(III) complex **3** was isolated in 2018 by Itoh et al. following oxidation of a bis(μ -hydroxo)dinickel(II) complex with hydrogen peroxide (Fig. 3).²⁰ The single crystal X-ray structure revealed a Ni–Ni distance of 2.863 Å, which is typical for other isolated μ -oxo Ni(III) dinuclear complexes. Notably, the Ni–O bond distances deviated largely from the previously reported values, which was attributed to the high mobility of the Ni₂O₂ core, resulting in an unexpected distortion. EPR spectroscopy showed half-field signals at $g = 4$, which indicated a triplet spin ground state. This assignment was further verified with SQUID from 2 K to 200 K, which showed paramagnetism across the temperature range due to the ferromagnetic coupling in the dinickel core.

Cyclam-based ligands have been shown to stabilize a unique ‘side-on’ peroxo binding mode to generate mononuclear Ni(III)-peroxo complexes. In 2009, the Nam group showed that a 12-membered tetramethylated cyclam ligand could be used along with H₂O₂ and triethylamine to generate the Ni(III) peroxo complex **4** (Fig. 4).²¹ An X-ray crystal structure of **4** clearly demonstrated the side-on binding of the peroxo ligand, resulting in a distorted octahedral geometry. The observed O–O bond length of 1.386 Å is longer than previously isolated Ni(II) superoxo complexes, which was attributed to the ‘side-on’ binding of the peroxo group. EPR spectroscopy of **4** in frozen MeCN exhibited a rhombic signal with g values of 2.22, 2.17, and 2.06, typical for the d^7 electronic

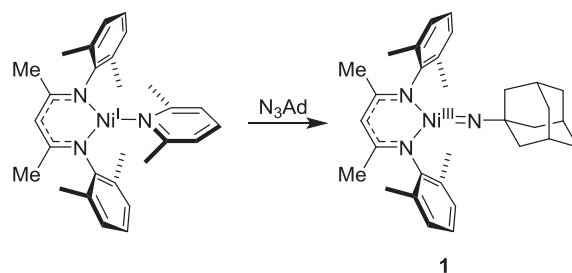


Fig. 1 Synthesis of a Ni(III)-imide complex **1**.

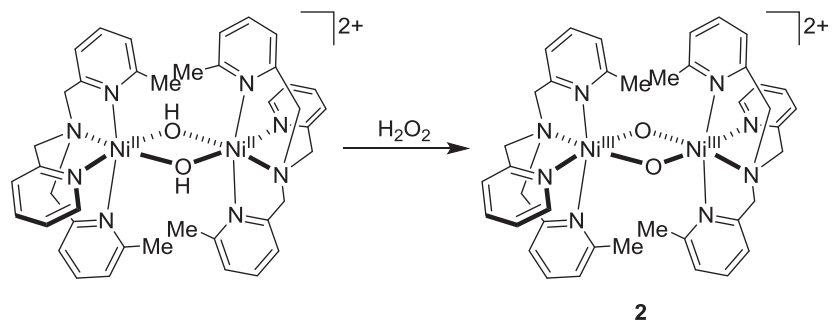


Fig. 2 Synthesis of the oxo-bridged dinuclear Ni(III) complex **2**.

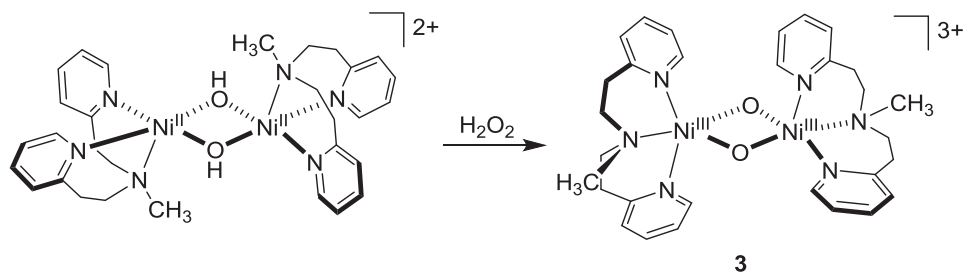


Fig. 3 Synthesis of oxo-bridged dinuclear Ni(III) complex **3**.

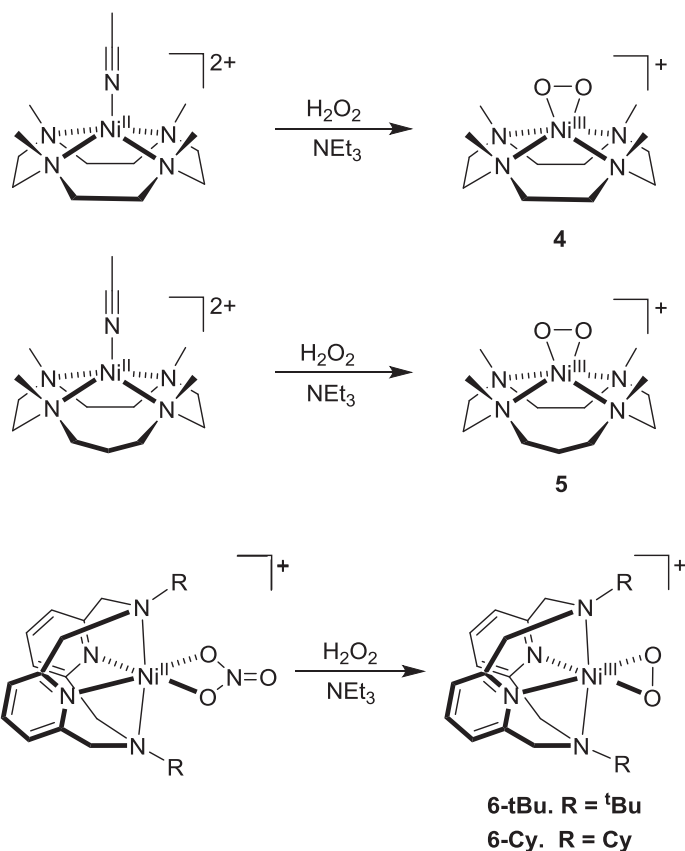


Fig. 4 Synthesis of side-on peroxo-Ni(III) complexes **4-6**.

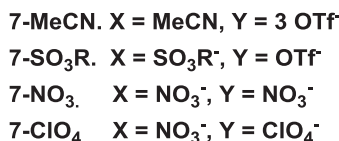
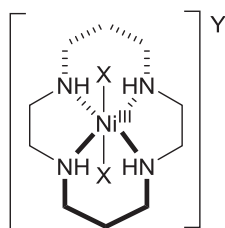


Fig. 5 Cyclam-supported Ni(III) complexes **7-X**.

configuration of Ni(III) complexes. Furthermore, the room temperature magnetic moment of the complex was determined to be $\mu_B = 2.13$, consistent with a $S = \frac{1}{2}$ ground state.

In 2013, the Nam group demonstrated that a 13-membered macrocyclic cyclam ligand could also be used to stabilize a side-on Ni(III)-peroxo complex **5** (Fig. 4).²² A single-crystal structure of **5** showed a distorted octahedral geometry with an O–O bond length of 1.384 Å, which is comparable to the bond distance observed in their previously reported Ni(III)-peroxo complexes. EPR spectroscopy of a frozen MeCN solution at 5 K exhibited an axial signal with g values of 2.19 and 2.07, and a room temperature magnetic moment of 2.1 μ_B is consistent with a $S = \frac{1}{2}$ ground state.

In 2015, Cho and coworkers reported that diazapyridinophane ligands also stabilize side-on Ni(III)-peroxo species binding, as demonstrated by complexes **6-tBu** and **6-Cy** (Fig. 5).²³ A single crystal X-ray structure of **6-tBu** revealed a distorted octahedral geometry with an O–O bond length of 1.401 Å, which is slightly longer than the previously reported Ni(III)-peroxo complexes described above. This elongation was attributed to the steric bulk of the *N-tert*-butyl groups of the ligand. The EPR spectrum of **6-Cy** in frozen MeCN at 20 K reveals an axial signal with g values of 2.19 and 2.02, suggesting a d_z^2 ground state, and a room temperature magnetic moment of 2.3 μ_B consistent with a $S = \frac{1}{2}$ ground state.

6.09.2.1.3 Ni-cyclam complexes

Macrocyclic cyclam-based ligands have been demonstrated to be successful for stabilizing other high-valent Ni(III) complexes. In 2012, Tatsumi et al. isolated complexes **7-MeCN** and **7-SO₃R** while attempting to build models of Methyl Coenzyme M reductase (Fig. 5).²⁴ A solid state EPR spectrum of **7-SO₃R** was obtained and revealed an axial signal with spin density residing primarily in the d_z^2 orbital on the Ni center, typical of $S = \frac{1}{2}$ octahedral d^7 complexes.

Shores et al. have also utilized cyclam ligands to synthesize a variety of Ni(III) complexes in 2018 (Fig. 5).²⁵ These complexes were some of the first examples of $S = 1/2$ Ni(III) species that exhibit single-molecule magnet behavior. The cationic nitrate and perchlorate complexes **7-NO₃** and **7-CIO₄**, respectively, were isolated and characterized by single-crystal X-ray diffraction and EPR spectroscopy.

6.09.2.1.4 Ni complexes with silyl-anilide ligands

Oxidative addition of methyl iodide to a Ni(I) silyl-amide complex yielding the Ni(III) complex **8** was demonstrated by Tilley et al. in 2013 (Fig. 6). This resulted in a rare example of a Ni(III)-alkyl complex, which was characterized through single crystal X-ray diffraction and EPR spectroscopy.²⁶ The X-ray structure of **8** revealed a T-shaped geometry, with a N–Ni–N bond angle of 167.4° and a Ni–C bond distance of 1.923 Å. The measured magnetic moment of $\mu_B = 1.78$ is consistent for a low spin d^7 complex with a single unpaired electron. EPR and DFT studies of **8** both placed the unpaired electron in a π^* orbital with significant metal character, with an observed anisotropic signal of $g_x = 2.32$, $g_y = 2.15$, and $g_z = 2.13$. Superhyperfine coupling to the two nitrogen atoms also indicated significant delocalization of unpaired spin density onto the nitrogen atoms, which agreed with the DFT-calculated HOMO for the molecule.

6.09.2.1.5 Ni complexes with macrocyclic N4 ligands

In 2014, a tetradentate diazapyridinophane N-donor ligand ^{tBu}N4 was used by Mirica et al. for the first time to isolate the Ni(III)-aryl halide complexes **9** (Fig. 7).³ Following oxidative addition to generate the Ni(II) species, treatment with FcPF₆ generated the

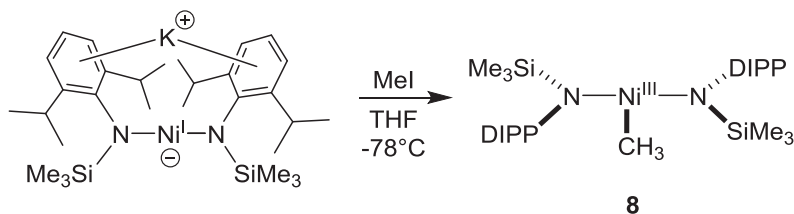


Fig. 6 The Ni^{III} methyl complex **8** stabilized by a silyl-anilide ligand.

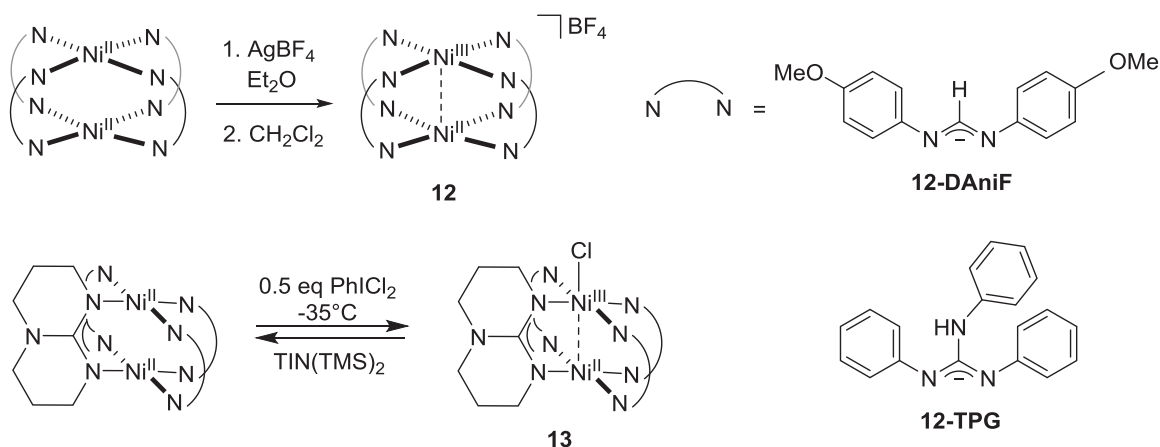


Fig. 8 Synthesis of the mixed-valent Ni(II)/Ni(III) dinuclear complexes **12–13**.

6.09.2.2 Ni Complexes With All-Carbon Ligands

6.09.2.2.1 Ni complexes with all-alkyl ligands

In 2009, a rare example of a tetra-alkyl Ni(IV) complex **14** was isolated by Nichols et al.⁸ The group utilized a strained bulky alkene (5*Z*,11*E*)-dibenzo[*a,e*]cyclooctatetraene that underwent ring opening metathesis after coordination to the Ni center (Fig. 9). The X-ray crystallography analysis of **14** revealed a highly distorted tetrahedral geometry at the metal center. Rather than the idealized C–Ni–C bond angles of 109.5° , four wide angles (122° – 129°) along with two narrow angles (80° – 81°) were observed. This distortion was attributed to the constraints of the 5-membered metallacycle. EPR spectroscopy and magnetic susceptibility indicated that the complex is diamagnetic, providing further confirmation that a Ni(IV) oxidation state is present.

Alonso et al. were also able to isolate homoleptic tetraarylphenyl Ni(III) complexes **15-F** and **15-Cl** by treating the corresponding dianionic Ni(II) precursors with different oxidants (Fig. 9).³¹ These complexes represent the first examples of homoleptic σ -organonickel(III) complexes and were characterized with X-ray crystallography and EPR spectroscopy. Notably, the crystal structure of **15-Cl** revealed a staggered conformation of the aryl rings, rendering the molecule chiral with a clockwise and anticlockwise

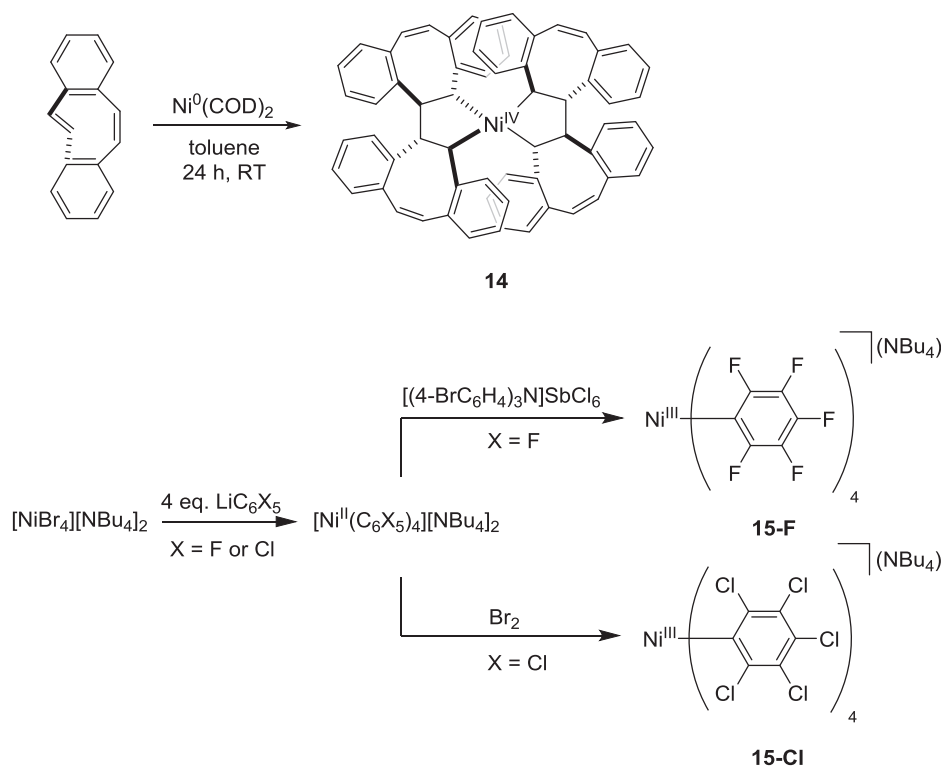


Fig. 9 Synthesis of Ni(III)- and Ni(IV)-tetraalkyl complexes **14** and **15**.

configuration. Low temperature EPR of complexes **15-F** and **15-Cl** reveals g_{\parallel}/g_{\perp} values of 1.910/2.940 and 1.935/2.874, respectively. Furthermore, the authors went on to determine that the unpaired electron exists primarily in the d_z^2 orbital by plotting g-perpendicular vs g-parallel.

6.09.2.2.2 Ni complexes with NHC-type ligands

In 2020, Anderson and coworkers crystallized a dinuclear nickel(III)-peroxo complex **16** by reacting dry oxygen with a Ni(II)-chloride precursor at -78°C (Fig. 10).³² The Ni–O bond length was found to be 1.834 Å, which is relatively short and indicative of a Ni(III) metal center. Its paramagnetic feature makes NMR resonance signals broad and shifted, but surprisingly the authors found it to be nearly EPR-silent due to unpaired electrons coupling. Further insight into this complex was gained by X-ray absorption spectroscopy. The Ni K-edge of the peroxo complex occurs higher than the chloro precursor by 0.7 eV, and EXAFS analysis of the peroxo complex suggested a fit of three carbon atoms and one oxygen atom in the first coordination sphere, consistent with a Ni(III) oxidation state.

6.09.2.3 Ni Complexes With Mixed Nitrogen-Oxygen Ligands

6.09.2.3.1 Ni complexes with Schiff base ligands

Schiff-base type ligand systems such as the salen ligands have seen widespread use in coordination chemistry in both transition metal catalysis and as ligands for stabilizing high-valent metal centers. In 2014, the Auffrant group isolated phosphasalensupported Ni(III) complex **17** following single electron oxidation of the Ni(II) precursor (Fig. 11).³³ The complex adopted a slightly distorted square-planar geometry, and a shortening of the Ni–O and Ni–N bonds from 1.875 to 1.842 Å and from 1.828 to 1.844 Å, respectively, was observed upon oxidation. The X-band EPR of complex **17** at 5 K revealed a large g-tensor anisotropy, with $g_1 = 2.29$, $g_2 = 2.215$, and $g_3 = 2.061$. The higher g_1 and g_2 values compared to g_3 indicated that there was predominant occupation of the unpaired electron in the xy plane, although with large degree of distortion due to the difference in values between g_1 and g_2 .

While investigating complexes with potential anti-cancer activity, Ay et al. isolated the Schiff-base supported Ni(III) complex **18** in 2020 (Fig. 11).³⁴ The authors found that the complex adopts a distorted octahedral geometry, which was attributed in part to the small bite angle of the 3-membered chelate ring of the acetate group. Although no further characterization was performed on the complex, it was found to have a cytotoxic effect on primary non-small lung cancer cells through an apoptotic pathway.

6.09.2.3.2 Ni complexes with pyridine-alkoxide ligands

Mixed nitrogen/oxygen ligands have also been used over the last 20 years for stabilizing high-valent nickel complexes. The dinuclear Ni(III) complex **19** was isolated by the Diao group in 2017 following oxidation of the dinuclear Ni(II) diacetate-bridged complex with $\text{PhNMe}_3\text{Br}_3$ (Fig. 12).³⁵ Surprisingly, a Br atom bridges the two Ni(III) centers and the Ni–Br–Ni bond angle was found to be 84.59° . Furthermore, dissociation of an acetate was observed causing it to coordinate κ^2 to one of the Ni centers.

In 2020 Brudvig et al. utilized 2-pyridinyl-2-propanoate ligands to synthesize a novel square planar Ni(III) complex **20** (Fig. 13). EPR studies of **20** showed a single $S = 1/2$ species, and a rhombic spectrum with $g_x = 2.077$, $g_y = 2.091$, and $g_z = 2.274$ confirmed the presence of a low-spin d^7 Ni(III) complex.³⁶ Attempts to crystallize complex **20** using pyridine as a co-solvent proved unsuccessful, however a DCM/pentane mixture allowed for the isolation of an octahedral complex with two axial pyridines and a PF_6^- counterion. Further EPR studies were performed on **20** and a rhombic signal with $g_x = 2.202$, $g_y = 2.163$, and $g_z = 2.030$ was observed along with a five-line superhyperfine coupling pattern, indicating coupling of the unpaired electron with the two pyridyl nitrogens.

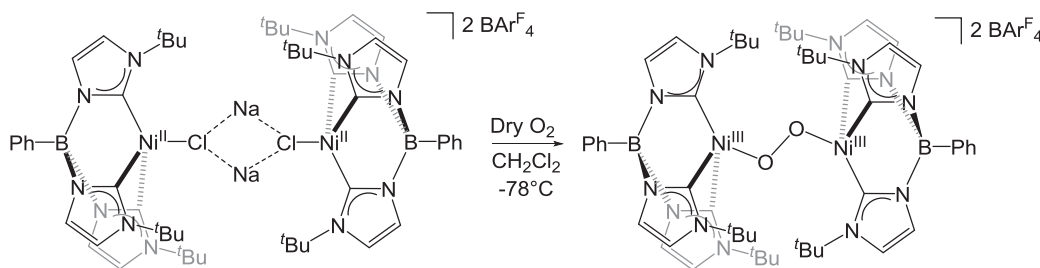


Fig. 10 Synthesis of a peroxo-bridged dinuclear Ni(III) complex **16**.

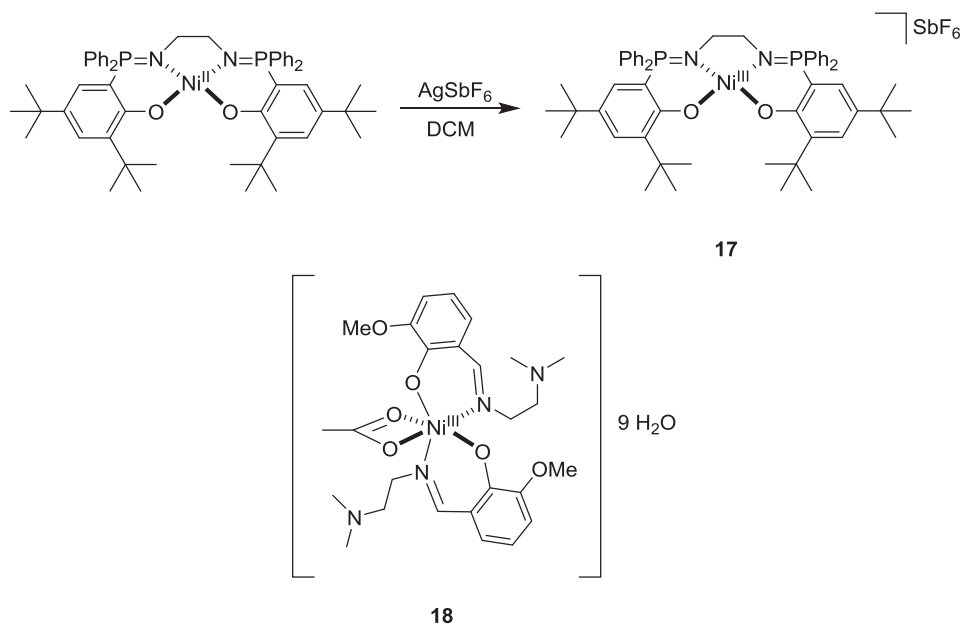


Fig. 11 Ni(III) Complexes supported by Schiff-base ligands.

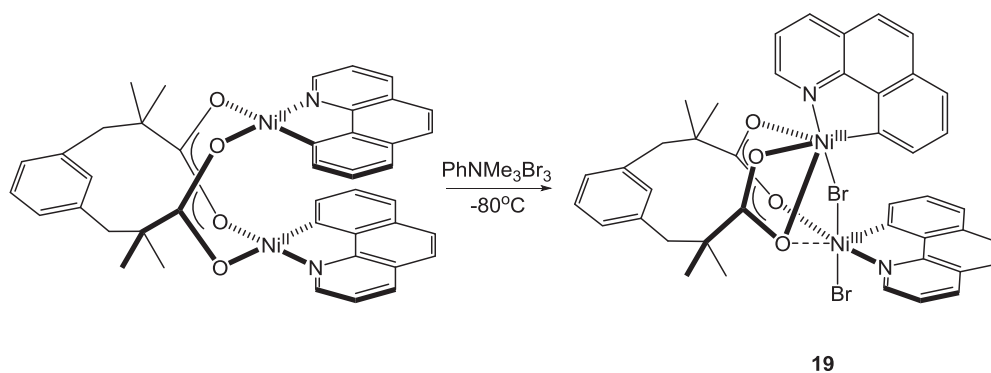


Fig. 12 Synthesis of the dinuclear Ni(III) complex 19.

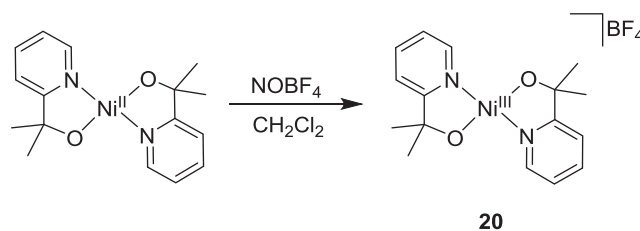
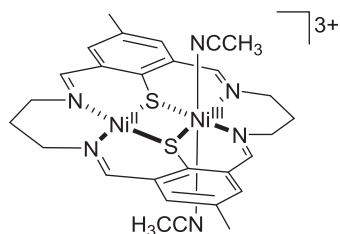


Fig. 13 Single electron oxidation to provide a square planar Ni(III) complex 20.

6.09.2.4 Ni Complexes With Mixed Nitrogen-Sulfur Ligands

6.09.2.4.1 Ni complexes with imine-thiolate ligands

The development of small molecule mimics of the $[\text{NiFe}]$ hydrogenase active site have led to the use of N/S-type ligands, and in 2008 the Lubitz group isolated a mixed-valent dinuclear Ni(II)/Ni(III) complex 21 utilizing such an approach (Fig. 14).³⁷ EPR measurements of the mixed-valent complex showed g values (2.035, 2.187, and 2.202), with a well-resolved quintet (1:2:3:2:1 intensity) in the g_z region. This splitting was attributed to the superhyperfine coupling with the axially coordinated acetonitrile ligands. Comparing the crystal structures of the Ni(II)/Ni(II) precursor to the oxidized Ni(II)/Ni(III) complex 21 revealed important



21

Fig. 14 The mixed-valent Ni(II)/Ni(III) complex **21** stabilized by a macrocyclic N/S-type ligand.

changes in the bond distances of the complexes, with the bond distance in **21** notably elongated compared to the Ni(II)/Ni(II) precursor. The average Ni–N and Ni–S bond distances in **21** were 1.954 Å and 2.2376 Å respectively, while the Ni(II)/Ni(II) precursor had values of 1.9165 Å and 2.176 Å.

6.09.2.4.2 Ni complexes with aza-thioether ligands

In 2011, McMaster and coworkers crystallized a series of Ni(III) complexes **22–24** with aza-thioether macrocycle ligands (Fig. 15). All of them adopt a six-coordinated distorted octahedral geometry, and compared to their Ni(II) precursors, each of them possesses shorter equatorial bond lengths due to the larger electrostatic attraction, and longer axial bond lengths due to Jahn-Teller distortion.³⁸ EPR spectroscopy confirms the presence of an unpaired electron in all these three Ni(III) complexes, and depending on the ligand identity, the frozen solution spectrum displays either axial or rhombic pattern at 77 K. In addition, from DFT calculations a good extent of charge delocalization from the Ni center to the S atoms was observed.

6.09.2.5 Ni Complexes With Mixed Phosphorus-Sulfur Ligands

6.09.2.5.1 Ni complexes with tris(thiolate)-phosphine ligands

The [NiFe] hydrogenase metalloenzyme catalyzes the two-electron oxidation of H₂ in aerobic and anaerobic organisms. To study the characteristics and reactivity of the Ni(III) intermediate proposed within this metalloenzyme, researchers have used a wide variety of P/S type ligands to build mimics of the enzyme active site. In 2006, the mononuclear Ni(III) complex **25** was isolated by Liaw et al. following oxidation of the Ni(II) thiol complex with dioxygen (Fig. 16).^{39,40} Complex **23** was characterized by paramagnetic ¹H NMR and SQUID magnetometry, which revealed a magnetic moment of 1.71 μ_B for this complex. These results supported the assignment of a low-spin d⁷ metal center with a distorted trigonal bipyramidal geometry, which was further confirmed through single crystal X-ray diffraction.

In 2008, the Liaw group went on to isolate a series of mononuclear Ni(III) complexes **26–29** utilizing a similar set of mixed sulfur/phosphorous-type ligands (Fig. 17).⁴¹ Chloro, phenoxide, and methoxide complexes were all analyzed via EPR, and exhibited rhombic signals with principal g values of g₁ = 2.28–2.34, g₂ = 2.04–2.09, and g₃ = 1.99–2.00. The higher g values of

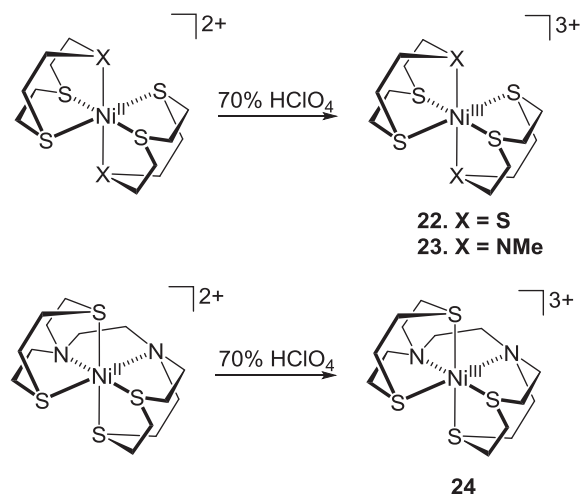


Fig. 15 Synthesis of complexes **22–24** using aza-thioether macrocyclic ligands.

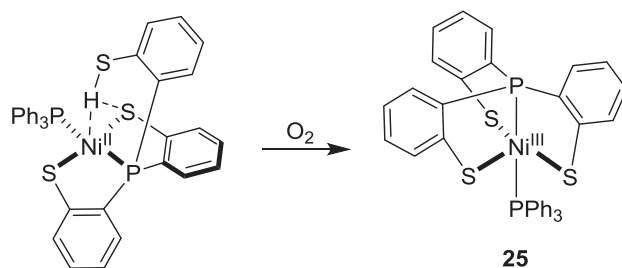


Fig. 16 Synthesis of complex **25**.

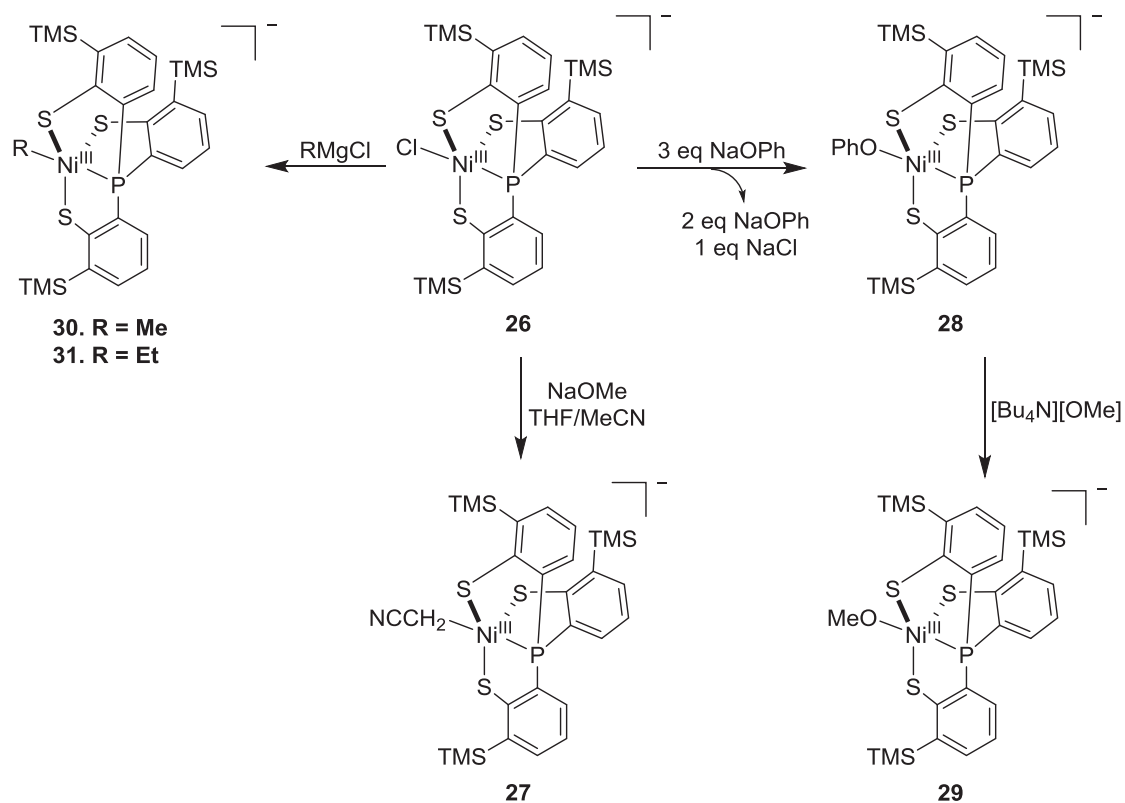


Fig. 17 Synthesis of a variety of tris(thiolate)phosphine complexes **26–31**.

26–29 compared to the free electron g value of 2.0023 indicated that the unpaired electron resides predominantly on the Ni center. Cyclic voltammetry studies were also conducted in MeCN for **26–29**, with each providing reversible peaks for Ni(II)/Ni(III) oxidation. The measured $E_{1/2}$ value of the complexes was found to be -1.20 , -1.26 , -1.32 , and -1.34 V respectively. The slight decrease throughout the series was attributed to the weaker electron donating ability of the coordinated ligand.

Using a similar platform, the Lee group isolated the first example of a Ni(III) methyl complex **30** along with the corresponding ethyl complex **31** in 2010 (Fig. 18).⁴² EPR analysis of the methyl complex **30** at 77 K displayed rhombicity with principal g values of 2.44, 2.00, and 1.96 respectively. The calculated g_{ave} of 2.13 indicated that the unpaired electron was found primarily on the nickel center, and further density functional theory calculations showed it occupied the d_{xy} and $d_{x^2-y^2}$ orbitals primarily. The authors compared their complex to the metalloenzyme methyl-coenzyme M reductase (MCR), which is thought to potentially contain a Ni(III)-methyl intermediate. EPR studies of the MCR active site reveal g_{\parallel} and g_{\perp} values of 2.22 and 2.10 respectively, which indicate that the unpaired electron resides primarily in the $d_{x^2-y^2}$ orbital of the Ni center.

Further reactivity studies on Ni(III) thiolate complexes were performed by Liaw et al. in 2013 and 2016, leading to the isolation of various insertion products **32**, **34**, and **35** (Fig. 18).^{43,44} Following treatment of the Ni(III) hydride complex with CS_2 , the insertion product compound **32** was obtained. At 77 K complex **32** showed a rhombic EPR spectrum with $g_1 = 2.28$, $g_2 = 2.03$, and

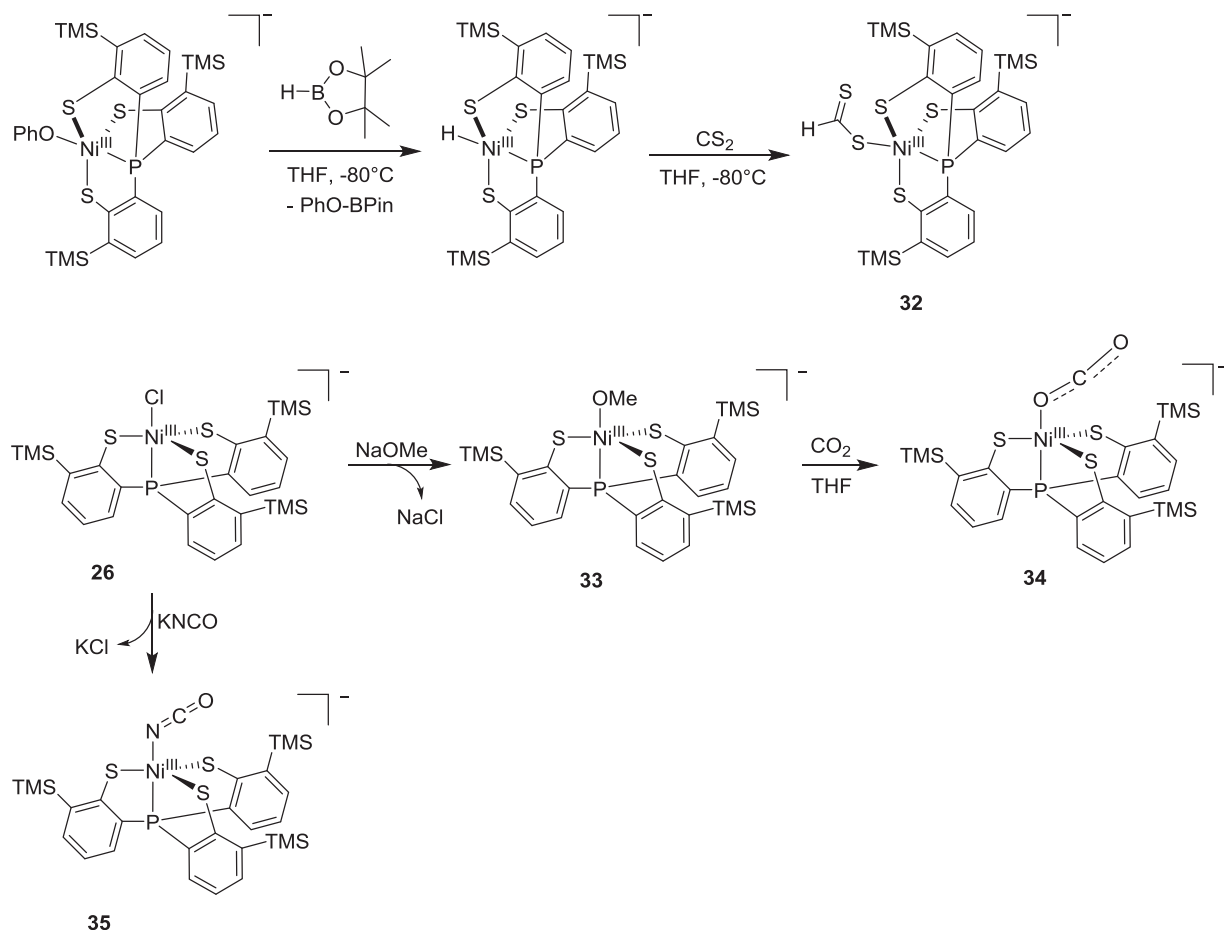


Fig. 18 Further reactivity studies with tris-thiolate Ni(III) complexes.

$g_3 = 1.99$. Along with X-ray crystallography, IR spectroscopy was also used to confirm the structure and that showed a distinct absorption at 1007 cm^{-1} , assigned to the asymmetric S=C vibration.

In a 2016 publication, the Liaw group observed a CO₂ insertion product **34** following bubbling of CO₂ into solution with complex **33** (Fig. 18). The formation of a methoxy radical which was captured by a spin-trapping reagent DMPO indicates that carbon dioxide binds to the metal center as a radical anion, maintaining a Ni(III) oxidation state. This assignment was further confirmed through X-ray crystallography, which revealed a bent O–C–O bond with a 171.7° bond angle and a significant difference in the individual O–C bond lengths (1.132 \AA vs 1.240 \AA). The EPR spectrum of complex **34** showed a combination of typical [Ni(III)(L)(PS₃)][−] complexes ($g_1 = 2.31$, $g_2 = 2.03$, $g_3 = 2.00$) along with a CO₂ radical anion contributing to the g anisotropy. Through spin quantitation using complex **35** as a reference, the authors concluded that the electronic structure of **34** is in resonance between a Ni(III)-CO₂ radical anion species and a Ni(II)-CO₂ adduct.

In 2007, the Liaw group used P/S type ligands to construct a series of dinuclear Ni(II)/Ni(III) complexes **36–38**, which were analyzed with UV-vis, EPR, and X-ray diffraction (Fig. 19).⁴⁵ Compared to complex **25**, the dimeric species indicates high rhombicity with principal g values of $g_1 = 2.113$, $g_2 = 2.073$, and $g_3 = 2.033$. A strong UV-Vis absorption at 1124 nm along with an extinction coefficient greater than $2000\text{ L mol}^{-1}\text{ cm}^{-1}$ was attributed to an inter-valence transition between the fully delocalized mixed-valent complexes in the dinuclear complex. The observed Ni–Ni distance in complex **36** was found to be 2.603 \AA , which increased to 2.829 \AA following reduction with NaBEt₃/KC₈. The increased bond distance was attributed to the SOMO of complex **37** having antibonding character for the Ni–Ni interaction. This elongation was not observed in complex **38** after treating **37** with [Me₃O][BF₄], for which a Ni–Ni distance of 2.609 \AA was observed.

6.09.2.5.2 Ni complexes with mixed phosphorus-thiolate ligands

Finally, P/S type ligands have also been successfully used to isolate Ni(IV) complexes. In 2018, Liaw et al. synthesized a neutral octahedral Ni(IV) complex **39** using a phosphine dithiophenol ligand (Fig. 20).⁴⁶ The authors were unable to analyze the complex using EPR spectroscopy, however, a single crystal X-ray structure was obtained. The cis-binding of the phosphine atoms resulted in a 102° bite angle, which is consistent with the general configuration among reported P₂S₄ complexes.

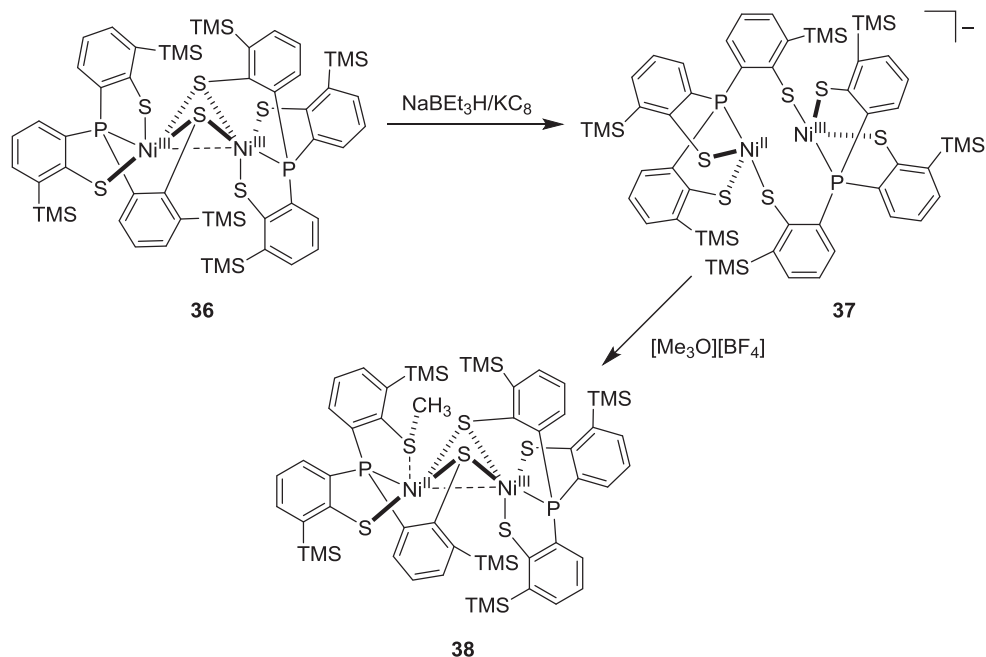


Fig. 19 Synthesis of dinuclear Ni(II)/Ni(III) complexes **36–38** using tris-thiolate phosphine ligands.

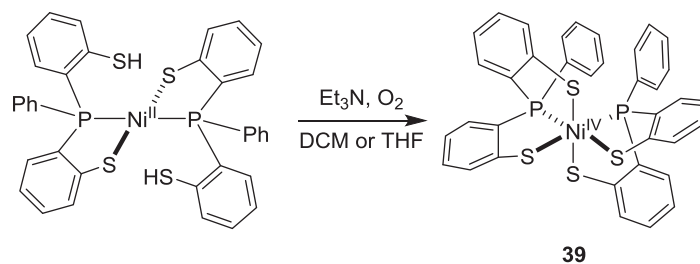


Fig. 20 A Ni(IV) complex **39** stabilized with tris-thiolate phosphine ligands.

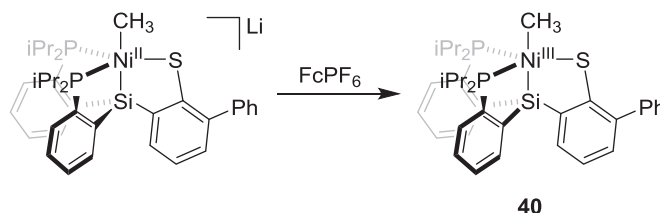


Fig. 21 Synthesis of a Ni(III)-methyl complex **40**.

In 2020 the Peters group isolated a P/S triarylsilane Ni(III)-methyl complex **40** while studying the hydrogen evolution from the related Ni(III)-hydride complex. X-ray crystallography revealed a trigonal bipyramidal structure, with a Ni–C bond distance of 2.047 Å and a Ni–Si bond distance of 2.2541 Å (Fig. 21).⁴⁷ The EPR spectrum of **40** revealed a rhombic g tensor ($g = 2.255, 2.073, 2.037$) with superhyperfine coupling to the two P atoms, and these values aligned with the in-situ EPR measurements for the analogous Ni(III) hydride complex.

6.09.2.6 Ni Complexes With Mixed Nitrogen-Carbon Ligands

6.09.2.6.1 Ni complexes with tris(2-pyridylthio)methanide ligands

Nitrogen-based ligands have seen widespread use in coordination chemistry and catalytic applications. The multiple functionalities and hybridizations of nitrogen allow for a large range of bonding opportunities for stabilizing a variety of high-valent coordination and organometallic compounds. A tris(2-pyridylthio)methanide ligand was used by Kinoshita et al. in 2011 for the synthesis of the dinuclear Ni(III) complex **41** upon oxidation of the dinuclear Ni(II) precursor. Treatment of complex **41** with acetonitrile or dichloromethane resulted in formation of a mononuclear Ni(III)-solvento complex **42** (Fig. 22).⁴⁸ This complex then underwent a novel rearrangement in which the N and S atoms of one of the pyridylthiolate arms exchange Ni- and C-bonding partners to form the N3S-coordinated organometallic Ni(III) complex **43**. This complex was then subjected to electrochemical reduction to regenerate the dinuclear Ni(II) precursor species, and thus reversing the observed ligand rearrangement.

6.09.2.6.2 Ni complexes with macrocyclic N₃C ligands

Starting in 2015, the Mirica group demonstrated that an ^RN₃C ligand with flexible tertiary amine arms could stabilize high-valent nickel complexes that can undergo aromatic methoxylation, hydroxylation, and cyanation transformations.^{49,50} Oxidation of the Ni(II) precursor with FePF₆ yielded the Ni(III) complex **44**, while a salt metathesis with TlSbF₆ followed by oxidation with FePF₆ in MeCN yielded Ni(III) complex **45** (Fig. 23). Both **44** and **45** displayed a distorted octahedral geometry, and magnetic moments of 1.68 and 1.71 μ_B. EPR spectra showed rhombic signals with g_{ave} values of 2.145 and 2.127 respectively. Superhyperfine coupling to the two axial N atoms was observed in the g_z direction in both complexes, along with superhyperfine coupling to the Br atom in **46** along the g_y and g_x directions.

The effects of substituents on the ^RN₃C ligand scaffold was then studied by Mirica et al. in 2016, leading to the isolation of a number of Ni(III) complexes **46–48** (Fig. 24), which exhibited uncommon aromatic cyanoalkylation reactivity through double C-H activation.⁵¹ A variety of complexes with different N-alkyl groups electron donating and withdrawing groups on the phenyl ligand backbone were synthesized, and the conformational and reactivity changes that occurred with this ligand variants were probed by EPR and X-ray crystallography.⁵²

6.09.2.6.3 Ni complexes with pyridine-aromatic amine ligands

In 2017 the Ritter group isolated a cationic Ni(III)-aryl complex **49** following oxidation of Ni(II) precursor with N-fluoropyridinium tetrafluoroborate (Fig. 25).⁵³ X-ray crystallography analysis revealed a distorted octahedral geometry, which agreed with the expected Jahn-Teller distortion for the d⁷ electronic configuration of **49**. EPR spectroscopy showed a rhombic signal with a g_{ave} value of 2.20, consistent with other 6-coordinate Ni(III) complexes.

Aminoquinoline-based ligands have seen widespread use in the field of C-H functionalization, and in 2019 Sanford et al. isolated a variety of organometallic aminoquinoline based Ni(III) complexes **50–51** to gain a better understanding of the mechanism of such reactions. Complex **50** was characterized by X-ray diffraction and EPR spectroscopy (Fig. 26).⁵⁴ The EPR spectra were

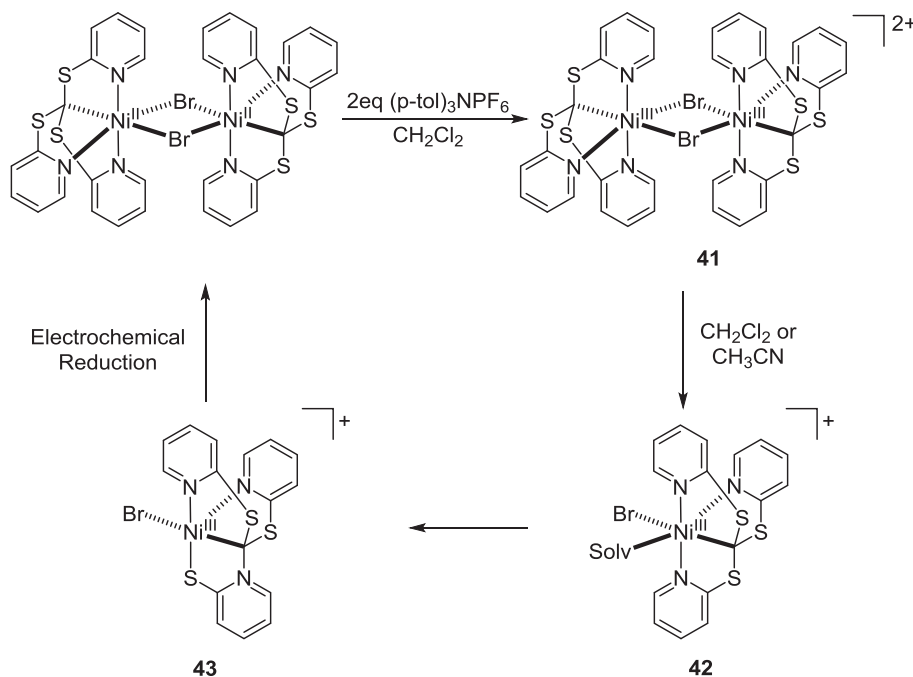


Fig. 22 A novel ligand rearrangement from complex **41** to **43**.

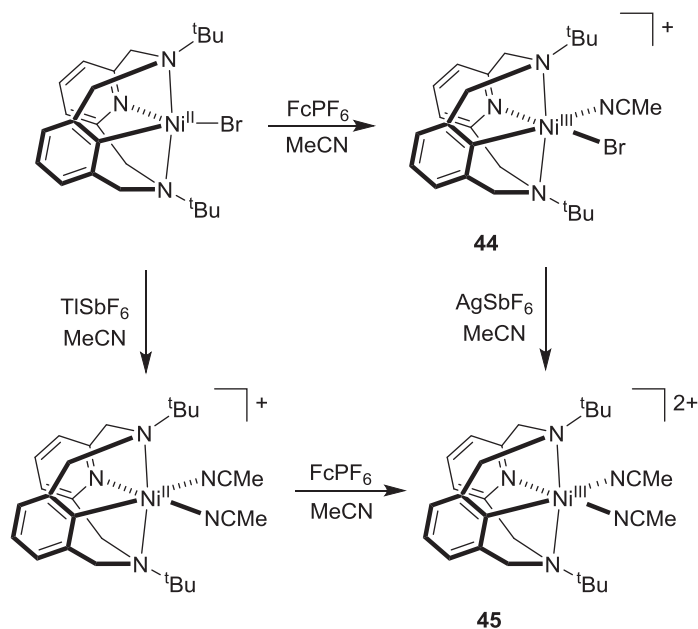


Fig. 23 Synthesis of complexes **44–45** using N_3C type ligands.

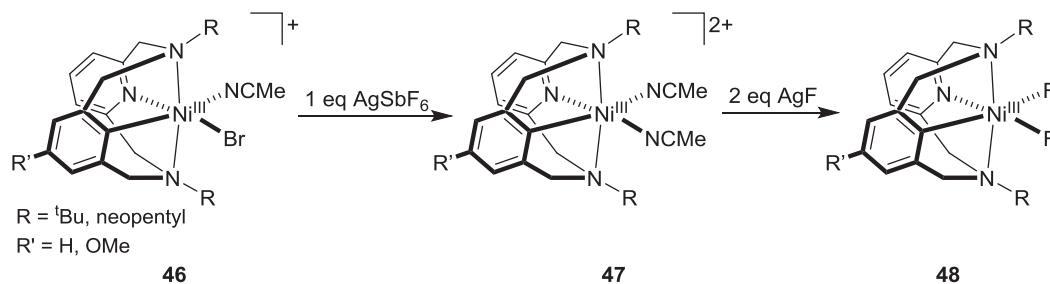


Fig. 24 Substituent variation on N_3C type ligands in complexes **46–48**.

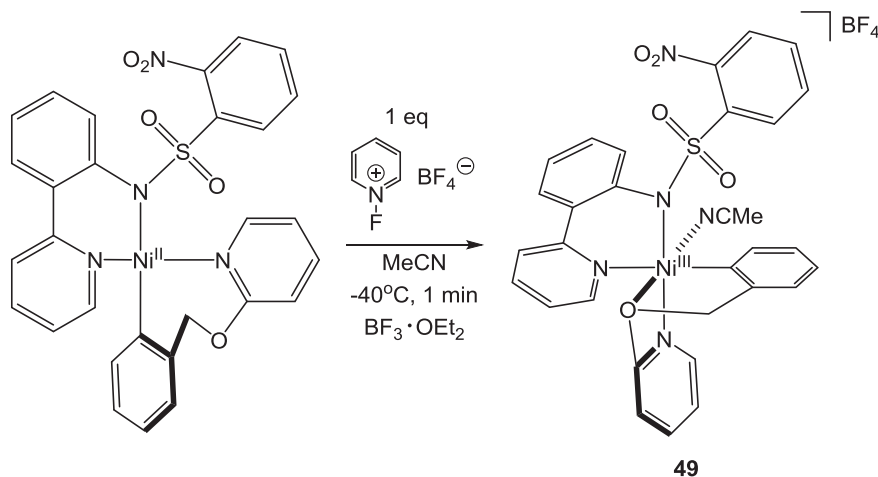


Fig. 25 One electron oxidation to form the distorted octahedral Ni(III) complex **49**.

consistent with a $S = \frac{1}{2}$ Ni(III) metal center, and the crystal structure showed a distorted square pyramidal geometry. The authors noted that the close proximity of the carboxylate ligand with the Ni metal center also could lead to coordination as a sixth ligand, however the Ni–O distance (2.628 Å) is large compared to the directly coordinated Ni–O bond distance of 1.954 Å, suggesting

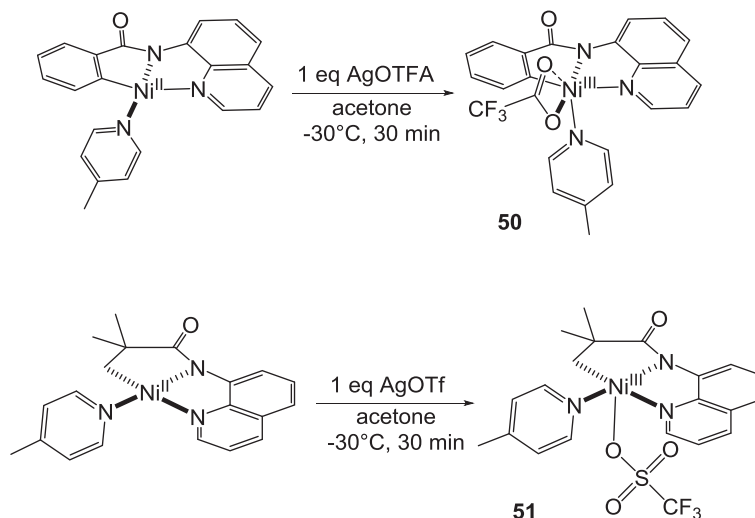


Fig. 26 Aminoquinoline-based Ni(III) complexes **50–51** isolated by the Sanford group.

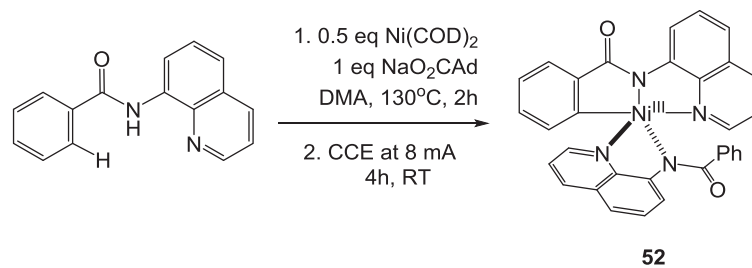


Fig. 27 Electrochemical generation of aminoquinoline Ni(III) complex **52**.

a weak interaction. Complex **51** was also characterized and similarly to **50**, the EPR spectra indicated a $S = \frac{1}{2}$ Ni(III) metal center, while the crystal structure showed a 5-coordinate square pyramidal geometry.

With a similar goal, the Ackerman group utilized electrochemistry to synthesize an aminoquinoline based Ni(III) complex **52** in 2020 (Fig. 27).⁵⁵ The structure of the complex was confirmed through X-ray crystallography, which showed a trigonal bipyramidal geometry. Furthermore, cyclic voltammetry was performed on the complex and a facile oxidation at 0.50 V vs. ferrocene indicated an oxidation event to a putative Ni(IV) species.

6.09.2.6.4 Ni complexes with tris(pyrazolyl)borate ligands

Biphenyl has shown to be an important ligand for probing the mechanism of $C_{sp^2}-X$ bond forming reactions, and the Sanford group has seen success in isolating high-valent Ni-biphenyl complexes by utilizing a tris(pyrazolyl)borate ligand. In a 2017 they reported the isolated Ni(IV) complexes **53** and **54** following oxidation of the Ni(II) precursor with bis(trifluoroacetoxy)iodobenzene (Fig. 28).⁵⁶ Treatment of this complex with $TMSCF_3$ along with a base activator generated the Ni(IV) complex **54**. Both of these complexes were characterized through X-ray diffraction and 1H , ^{13}C , ^{11}B , and ^{19}F NMR spectroscopy.

While investigating the aryl-fluoride bond formation from Ni(IV) metal centers, Sanford et al. isolated the organometallic Ni(IV) aryl-fluoride complex **55** in 2019 (Fig. 28).⁵⁷ This complex was characterized through 1H , ^{19}F , and ^{11}B NMR spectroscopy, along with X-ray diffraction. A diagnostic metal-fluoride ^{19}F NMR shift of -423.0 ppm along with the X-ray crystal structure confirmed the diamagnetic octahedral Ni(IV) structure.

6.09.2.7 Ni Complexes With Pincer Ligands

6.09.2.7.1 Ni complexes with POCOP pincer ligands

Over the last two decades, pincer ligands have emerged as powerful tools for stabilizing high-valent coordination compounds. The rigidity of the ligand framework results in high thermal stability, due largely to the inhibition of cyclometallation of the organic substituents. The variability of pincer complexes has led to a wide variety of phosphine, amine, and oxygen-based ligand frameworks, many of which are discussed below.

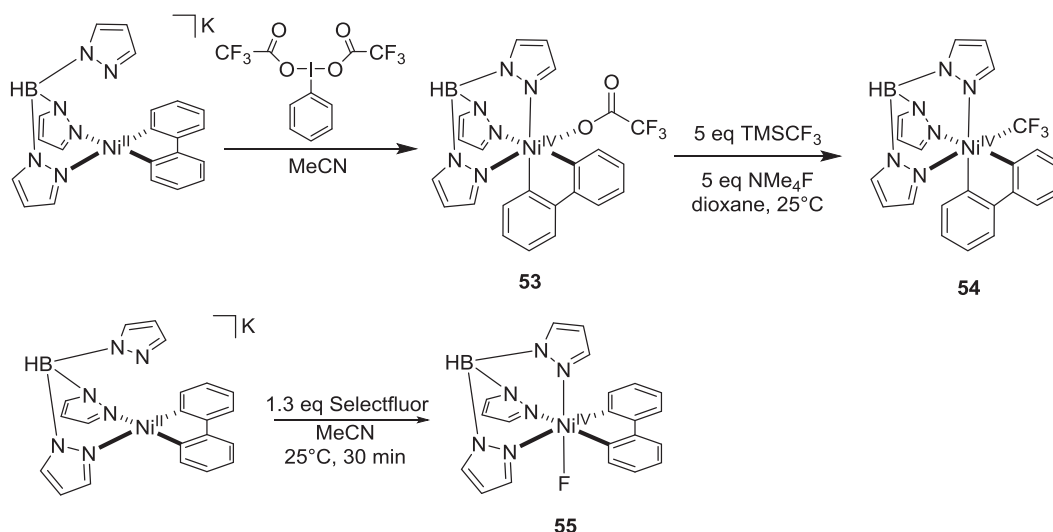


Fig. 28 Organometallic Ni^{IV} biphenyl complexes **53–55**.

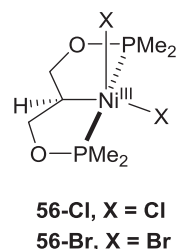


Fig. 29 A POCOP-type pincer ligand used to stabilize complexes **56**.

In 2007 Zargarian et al. isolated the organometallic Ni(III) dihalide complexes **56** utilizing a POCOP-type pincer ligand. X-ray crystallography revealed a square-pyramidal geometry, with the Ni metal center slightly out of plane of the pincer ligand (**Fig. 29**).⁵⁸ A relatively large difference was also observed in the Ni-X bond lengths (2.26 Å vs 2.32 Å for Cl and 2.37 Å vs 2.44 Å for Br, respectively), which was proposed to result from partial occupation of the p_z/d_z^2 Ni orbitals.

6.09.2.7.2 Ni complexes with POCN pincer ligands

Aryl POCN-type asymmetric pincer ligands with various N-substituents were used in 2009 by Zargarian et al. to isolate the organometallic Ni(III)-dibromide complex **57**. The square-pyramidal geometry of this complex was confirmed through single crystal X-ray diffraction, with slight pyramidal distortion due to an out-of-plane Ni metal center (**Fig. 30**).⁵⁹ The EPR spectrum of **57** was typical of Ni(III) pincer complexes with an axial g-tensor and superhyperfine coupling to the halogen atom on the g_z component.

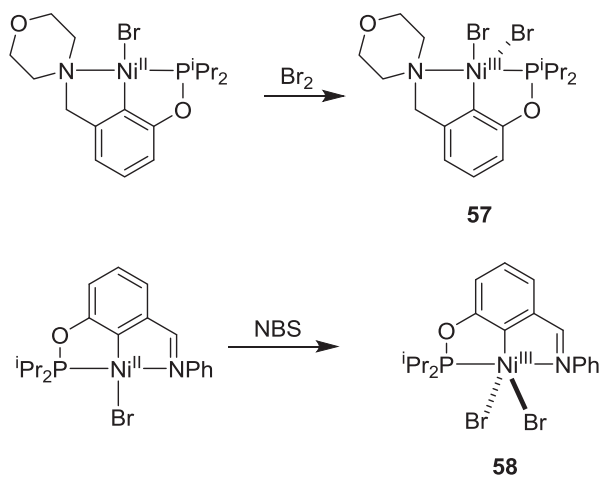


Fig. 30 Synthesis of complexes **57–58** using POCN-type ligands.

The g_z value was measured to be close to the free electron value (2.0023), while the g_x and g_y components were ~ 2.200 , which is typical for low-spin d^7 complexes. The same group went on to isolate a similar POCN Ni(III)-dibromide complex **58** in 2014 through treatment of the monohalide Ni(II) complex with NBS.⁶⁰ Structurally, the complex resembled previous trivalent pentacoordinate Ni species that had been isolated, however there was a slight modification by inclusion of an imine rather than a tertiary amine. A trigonal bipyramidal geometry with a slight pyramidal distortion due to displacement of an out-of-plane Ni atom was present, along with an elongated axial Ni–Br bond (2.45 Å axial vs 2.36 Å equatorial Ni–Br bond lengths).

6.09.2.7.3 Ni complexes with PCN pincer ligands

In 2018, Wendt and coworkers isolated Ni(III)-dichloro and -dibromo complexes **59–60** with the PCN-type ligand 1-(3-((*di*tert-butylphosphino)methyl)-phenyl)-*N,N*-dimethyl-methanamine, for which the stability of complexes is enhanced by implementing bulky *tert*-butyl groups on the phosphine atom (Fig. 31).⁶¹ In both crystal structures the Ni center adopts a five-coordinated distorted square pyramidal geometry, with one halide at the apical position. The longer bond length along the axial direction (Ni–Cl = 2.289 Å, Ni–Br = 2.443 Å) was caused by the nature of such complex, and in line with the EPR studies at 20 K that reveal rhombic signals, indicating a Ni(III) center bearing an unpaired electron in a d_z^2 ground state.

6.09.2.7.4 Ni complexes with NCN pincer ligands

NCN-type pincer ligands have seen success in stabilizing a variety of mono and dihalide Ni(III) complexes, and a mixed halide complex **61** was synthesized by Kozhanov et al. in 2009 through treatment of the monohalide complex with anhydrous copper halide salts (Fig. 32).⁶² The authors found that the EPR spectra of complex **61** was a superposition of two different isomers (Fig. 32). Although the complex isomerizes in solution, the authors noted that only the isomer with the bromide in the axial position was found in the solid state.

In 2019, Zargarian and coworkers successfully stabilized the related Ni(III)-dibromide complex **62** using the same NCN-type pincer ligand. This led to the isolation of a distorted octahedral tris(acetonitrile) Ni(III) complex **63**, and another Ni(III) square pyramidal complex **64** supported by a single acetonitrile and bromide via addition of appropriate amount of silver ions (Fig. 32).⁶³ Complex **63**, being air-stable despite possessing 19 valence electrons, exhibits a significant distortion along the z -axis likely due to the localized unpaired electron in Ni d -based orbitals, as confirmed by EPR. The five-coordinated complex **64** has 17 valence electrons, and its EPR studies at 120 K reveal the coexistence of two isomers in a solution, in which the bromine

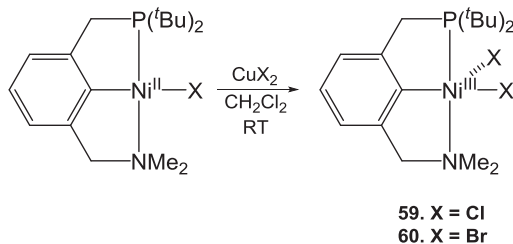


Fig. 31 Dihalide-Ni(III) complexes **59–60** stabilized by a PCN pincer ligand.

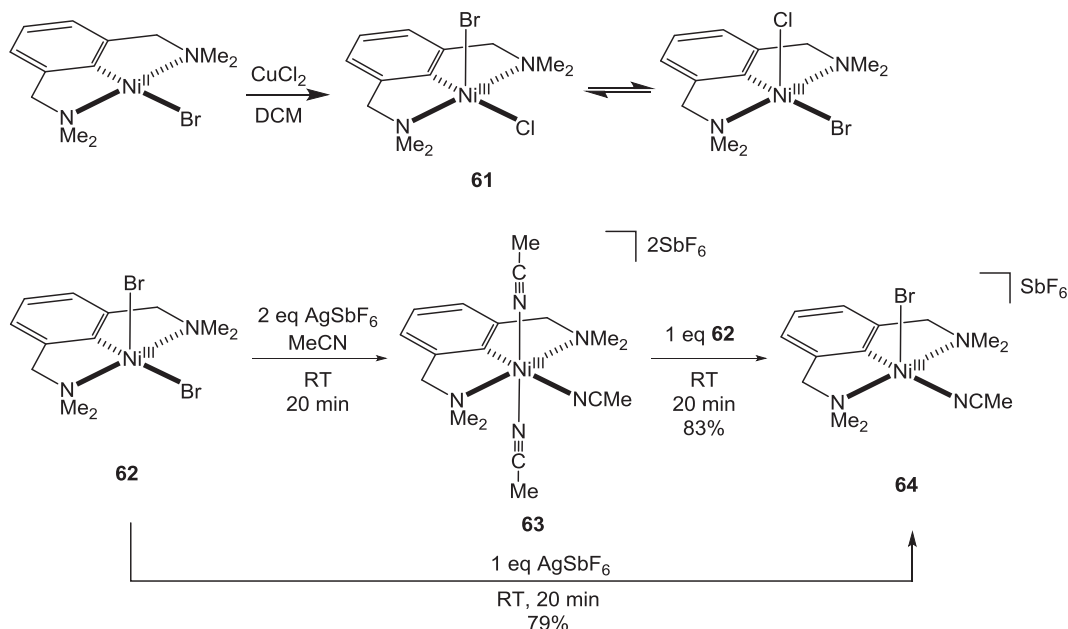


Fig. 32 An NCN-type pincer ligand was used to stabilize various Ni(III) complexes **61–64**.

atom resides in either the axial position or in the equatorial plane. The crystallized structure exists predominantly with the bromine in the axial position, and an energy difference ~ 4 kcal/mol was calculated between the two isomers.

6.09.2.7.5 Ni complexes with NHC pincer ligands

In 2016 the Fout group hypothesized that a NHC-based CCC pincer Ni(III) complex could be generated following single-electron oxidation of the Ni(II) precursor. However, treatment of with PhICl_2 generated a diamagnetic complex **65**, which was then further characterized with X-ray diffraction to reveal an octahedral trichloride Ni(IV) complex (Fig. 33).⁶⁴ Encouraged by these results they sought to also isolate the tri-bromide complex **66**, which was achieved through treatment of the Ni(II) bromine precursor with Br_2 or BTMABr_3 and subsequently characterized by X-ray diffraction, and was also shown to promote bromination of exogenous alkenes.

6.09.2.8 Ni Complexes With Perfluoroalkyl Ligands

Perfluoroalkyl groups have emerged as popular ligands for stabilizing high-valent organometallic Ni complexes, largely due to their reduced rate of reductive elimination. In 2015, Vicic and coworkers utilized a combination of octafluorobut-di-yl along with the terpyridine ligand to isolate an organometallic Ni(III) complex **67** following oxidation of the corresponding Ni(II) species with AgBF_4 (Fig. 34).⁶⁵ Inclusion of the C_4F_8 ligand was key in isolating this complex, as the corresponding bis(trifluoromethyl) complex was unstable under ambient conditions. X-ray crystallography of **67** confirmed an octahedral geometry, with notable elongation of the Ni–N bonds *trans* to the fluoroalkyl groups (2.163 Å and 2.172 Å) compared to the *cis* bonds (1.966 Å and 1.964 Å). This elongation was attributed to the accumulation of spin density on the *cis*-bound nitrogen and is characteristic of ligands bound *trans* to trifluoroalkyl ligands. Indeed, variable temperature solution and solid phase EPR spectra revealed superhyperfine splitting from two nitrogen atoms. This was confirmed by DFT calculations, which showed minimal spin density surrounding the central nitrogen of the terpyridine ligand and the axially coordinated acetonitrile.

The same octafluorobut-di-yl ligand was used by the Vicic group in 2018 to generate a stable Ni(IV)-difluoride complex **68** (Fig. 35).⁶⁶ The complex adopted an octahedral geometry with the two fluorides *trans* to each other, therefore possessing a C_2 symmetry, which was confirmed through characterization by ^1H and ^{19}F NMR spectroscopy.

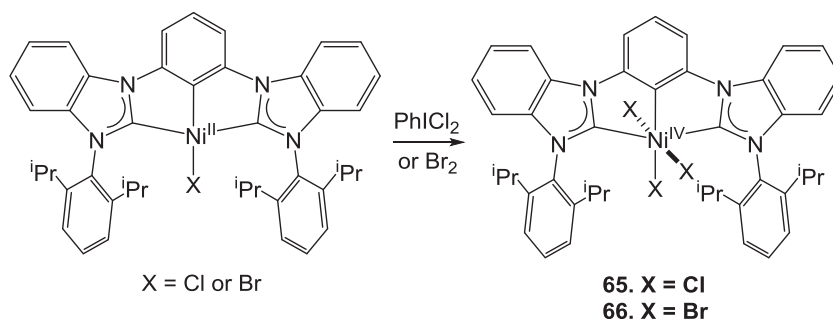


Fig. 33 Synthesis of a NHC pincer trihalide Ni^{IV} complexes **65–66**.

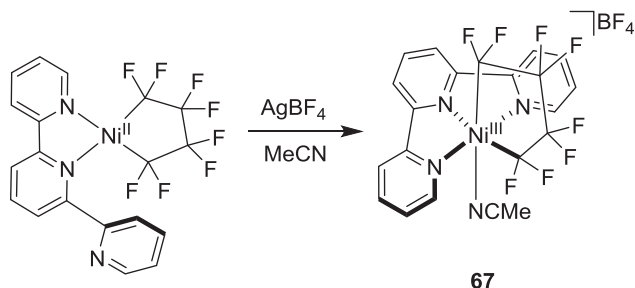


Fig. 34 Synthesis of complex **67** using terpyridine and octafluorobut-di-yl ligands.

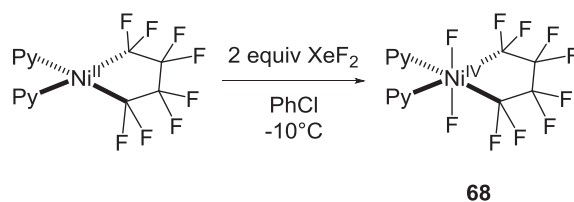


Fig. 35 Synthesis of Ni(IV) complex **68**.

In 2015 Mirica et al. isolated a stable bis(trifluoromethyl) Ni(III) complexes **69** and **70** utilizing a tetradentate N-donor ligand R^N4 . Both the Me^N4 and tBu^N4 complexes displayed a distorted octahedral geometry and bond distances that matched previously reported (tBu^N4)Ni(III) complexes (Fig. 36).⁶⁷ The paramagnetic complexes **69** and **70** had effective magnetic moments of 2.06 and 2.15 respectively, indicating a single unpaired electron. EPR spectroscopy revealed g_{ave} values of 2.105 and 2.143 respectively, confirming a Ni(III) metal center with a d_{z^2} ground state. Furthermore, superhyperfine coupling to the axial nitrogen atoms was observed in the g_z direction for both complexes.

In the same year, Sanford et al. performed a two-electron oxidation of the Ni(II)-aryl trifluoromethyl complex **71** with 5-(trifluoromethyl)dibenzothiophenium triflate (TDTT) to generate the Ni(IV)-aryl bis(trifluoromethyl) complex **72** (Fig. 37).⁶⁸ This represented one of the first examples of a two electron oxidation of a Ni-trifluoromethyl complex, and the corresponding Ni(IV) compound **72** was characterized through 1H , ^{13}C , ^{11}B , and ^{19}F NMR spectroscopy along with X-ray crystallography, which revealed an octahedral geometry around the Ni center.

In 2017, the Sanford group went on to isolate a series of Ni(IV) trifluoromethyl complexes **73–76** through a two-electron oxidation of Ni(II) precursors with N-fluoro-2,4,6-trimethylpyridinium (NFTPT, Fig. 38).⁶⁹ Along with X-ray crystallography, ^{19}F NMR was used to confirm the presence of a new Ni(IV) species. A significant downfield shift (-182 ppm from -138 ppm) was observed

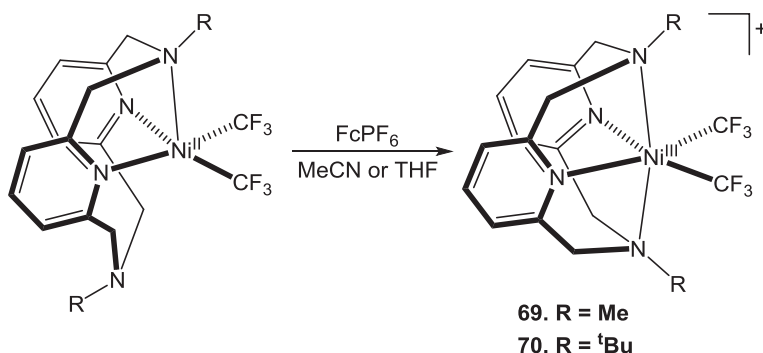


Fig. 36 Synthesis of Ni(III)(CF₃)₂ complexes **69–70** using R^N4 ligands.

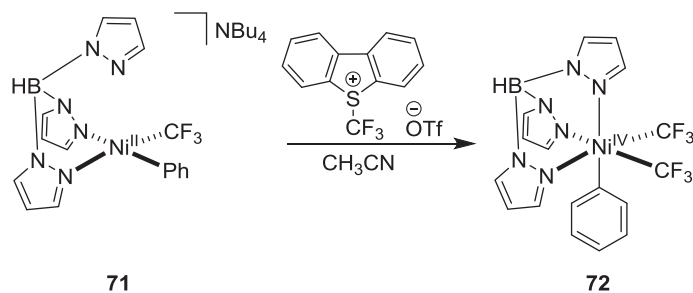


Fig. 37 Synthesis of the Ni(IV)-aryl bis(trifluoromethyl) complex **72**.

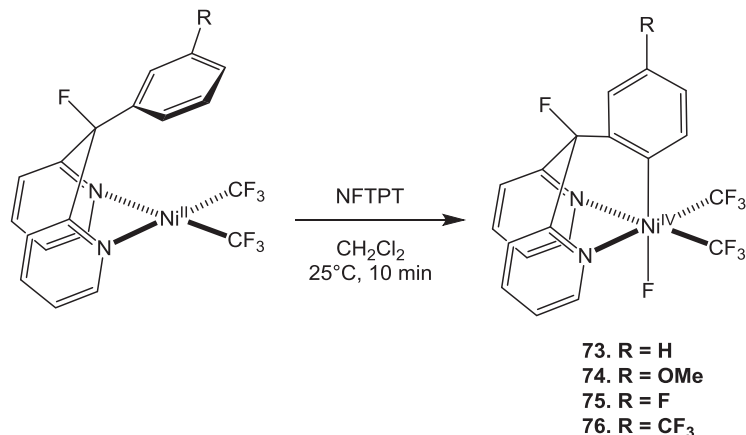


Fig. 38 Synthesis of complexes **73–76**.

for the fluorine atom bound to the ligand framework for complexes **73** to **74**, and the trend was also observed for the other complexes in the series with more electron deficient phenyl rings.

Nebra et al. observed that oxidation of a Ni(II) bis(trifluoromethyl) complex with one equivalent of XeF₂ led to the formation of the fluorine bridged dinuclear Ni(III) complex **77** (Fig. 39).⁷⁰ Addition of pyridine caused a reversible dissociation of **77** to the mononuclear Ni(III) complex **78**. Complexes **77** and **78** were confirmed through X-ray diffraction along with EPR spectroscopy. Complex **77** exhibits *g* values *g_x* = 2.237, *g_y* = 2.166, *g_z* = 2.018, while complex **78** has *g* values of *g_x* = 2.232, *g_y* = 2.166, *g_z* = 2.018. Furthermore, superhyperfine coupling to a single F atom was observed for **77**. Treatment of the Ni(II) bis(trifluoromethyl) precursor with two equivalents of XeF₂ generated the mononuclear Ni(IV)-difluoride complex **79** in up to gram quantities. ¹⁹F NMR of this complex revealed a triplet signal at −26.1 ppm (CF₃) and a septuplet at −418.3 (F), indicating two equivalent CF₃ and fluoride ligands. The spectroscopic data along with an X-ray crystal structure confirmed the assignment of a Ni(IV) metal center in **79**, which is a rare example of a Ni(IV) complex that is not supported by a multidentate chelating ligand.

The unique stabilizing effects of perfluorinated organic ligands have made them highly successful for isolating various high-valent Ni complexes. In 2019, a series of organometallic Ni(IV) complexes **80–82** were isolated by Sanford et al. utilizing a bpy-tBu-F ligand, and these complexes were shown to undergo C–H bond activation and subsequent functionalization following oxidation of the Ni(II) precursor with NFIPt (Fig. 40).⁷¹ These complexes were isolated and single crystal X-ray structures along with ¹⁹F and ¹H NMR spectra were obtained. Using the ligand fluorine as a spectroscopic tracking measurement, oxidation of the Ni(II) precursor with NFIPt generated two new F signals at −178 and −176 ppm in a ~1:4 ratio. Furthermore, a new singlet at −242 ppm was observed, indicating formation of a new Ni–F bond which was then confirmed through single crystal X-ray spectroscopy. ¹H NMR was also performed on the crude reaction to confirm a C–H bond activation event, and the spectra showed two new singlets at 3.87 and 3.41 ppm in a 1:4 ratio, confirming formation of the Ni–C bond. Treatment of this reaction solution with TMSCl followed by an aqueous NaCl solution lead to the formation of **81**, which was subsequently characterized with ¹H, ¹⁹F, ¹³C and X-ray crystallography. Further reaction of **81** with excess AgF generated the corresponding Ni(IV)-fluoride complex **82**.

In the same year, the Sanford group went on to expand on the reactivity of high-valent Ni complexes by reacting the Ni(III) precursor **83** with a variety of radical species to generate the corresponding Ni(IV) compounds **84–86** (Fig. 41).⁷² X-ray crystallography of the Ni(III) starting material **83** confirmed a five-coordinate geometry, which was further validated through EPR spectroscopy (*g_x* = 2.28, *g_y* = 2.22, and *g_z* = 2.01). Superhyperfine coupling to a single N atom of one of the pyrazole ligands was also observed. Oxidation of this complex with a variety of peroxides generated complexes **84–86**, each of which were characterized through single crystal X-ray diffraction to confirm their octahedral structure.

Sanford et al. isolated an organometallic Ni(IV) tris(trifluoromethyl) complex **87** through oxidation of the Ni(II) precursor with a fluorinated TDTT analog (Fig. 42).⁷³ The complex proved exceptionally stable to ambient conditions in the solid state and was characterized through ¹H, ¹⁹F, ¹³C, and ¹¹B NMR spectroscopy along with X-ray diffraction.

Lastly, Vivic and coworkers were able to isolate a formally Ni(IV) complex **88** by oxidizing the corresponding [Ni^{II}(CF₃)₄]^{2−} precursor with potassium persulfate (Fig. 43).⁷⁴ The Ni(IV) center in **88** is ligated to four CF₃[−] groups, with Ni–C bond lengths 2.021(6) and 1.942(6) Å, while a sulfate group binds in a bidentate fashion with Ni–O bond lengths of 1.964(4) Å, thus creating an overall dianionic complex. Interestingly, this complex is another example of a Ni(IV)-trifluoromethyl complex that is not supported by any chelating multidentate ligand.

6.09.2.9 Ni Complexes With Cycloneophyl Ligands

The cycloneophyl ligand has become a powerful tool for coordination chemists to isolate high-valent metalacycle complexes. This bidentate C-donor ligand generates complexes with exceptional stability due to the reduced rates of reductive elimination and inability to undergo beta-hydride elimination. The Sanford group has employed this ligand in a number of publications in the last 10 years, largely to stabilize Ni(IV)-trifluoromethyl complexes. In 2015, the group utilized S-(trifluoromethyl)dibenzothioephene triflate (TDTT) as an oxidant and isolated an organometallic Ni(IV) complex **89** (Fig. 44).⁴ Through X-ray diffraction they

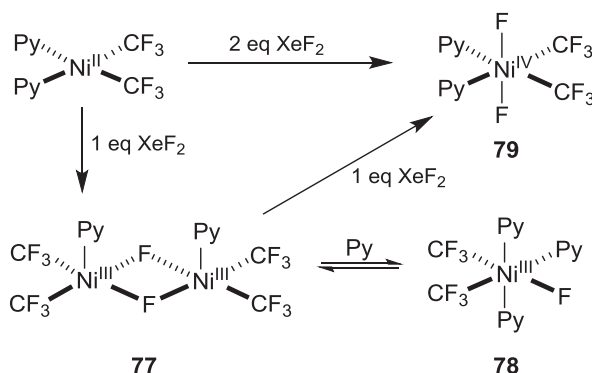


Fig. 39 Synthesis of high-valent Ni bis(trifluoromethyl) complex **77–79**.

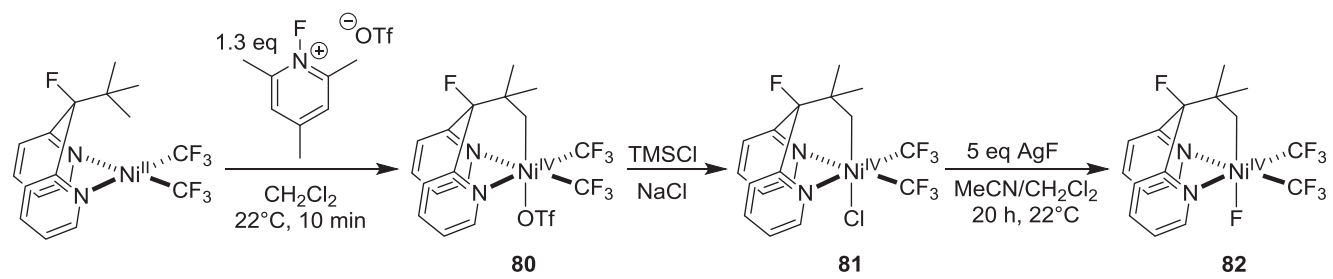


Fig. 40 C–H Bond activation leading to the synthesis of Ni(IV) complexes **80**–**82**.

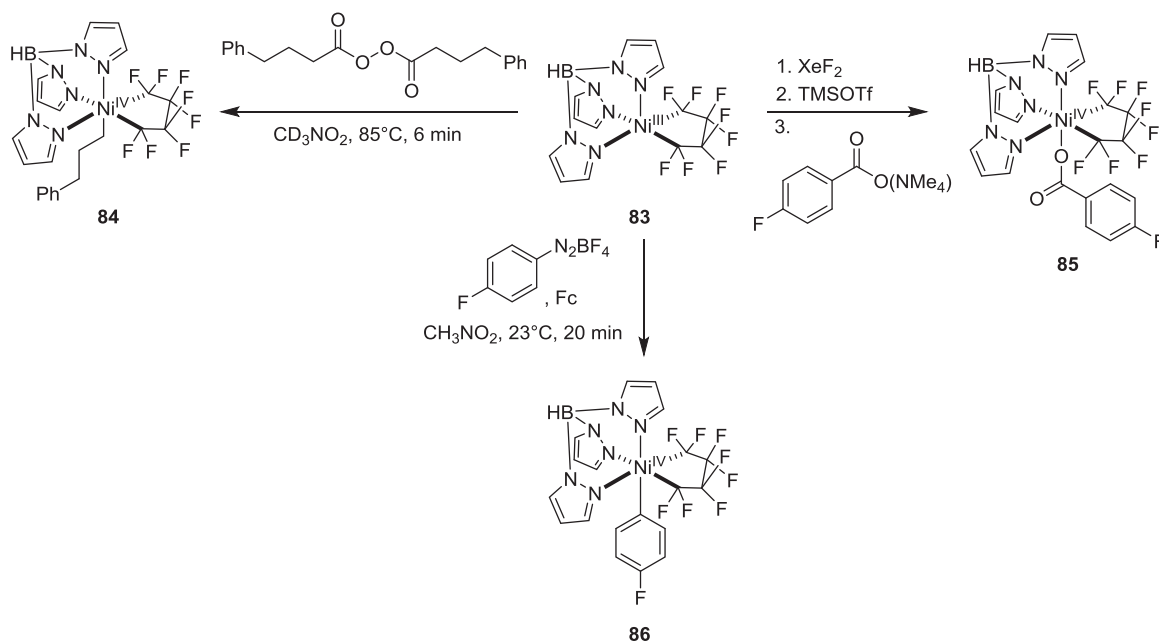


Fig. 41 Synthesis of various Ni(III) complexes **84**–**87** via radical reactions from a Ni(III) precursor.

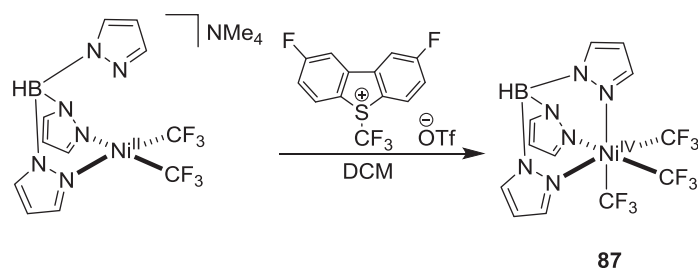


Fig. 42 Synthesis of complex **87** via a two-electron oxidation of a Ni(II) precursor.

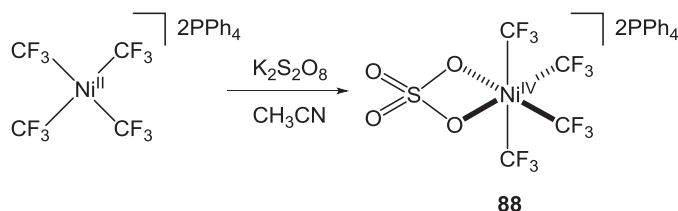


Fig. 43 Synthesis of an unsupported Ni(IV)-tetrakis(trifluoromethyl) complex **88**.

were able to confirm an octahedral geometry at the Ni center, making it the second isolable organometallic octahedral Ni(IV) complex at the time. In 2017, the group went on to generate complex **90** by using a trispyrazolylborate ligand rather than a tripyridine scaffold. The complex was characterized through ¹H, ¹³C, ¹¹B, and ¹⁹F NMR along with X-ray crystallography, which confirmed the octahedral geometry of the complex.

Starting in 2014, the Mirica group has used the macrocyclic pyridinophane ^RN₄ ligands to stabilize a series of high-valent Ni complexes, including cycloneophyl complexes. In 2016 they reported the (^{Me}N₄)Ni^{III}(cycloneophyl) complex **91**, which was formed upon oxidation of the Ni(II) precursor with FcPF₆.²⁷ Interestingly, complex **91** can be further oxidized with NOPF₆ to yield the Ni(IV) complex **94**, which was isolated and characterized by ¹H and ¹³C NMR and X-ray photoelectron spectroscopy (XPS). This ligand system represents the first reported ligand system to allow the synthesis of both Ni(III) and Ni(IV) complexes. In 2019 the same group reported the use of ^RN₄ ligands with one or two N-tosyl groups to generate the Ni(III) complexes **92** and **93**. Complex **92** was characterized through EPR spectroscopy, which revealed a rhombic signal with superhyperfine coupling in the g_z direction due to a single axial N donor (**Fig. 45**).⁷⁵ The presence of superhyperfine coupling to only one axial nitrogen suggested that the N_{Ts}

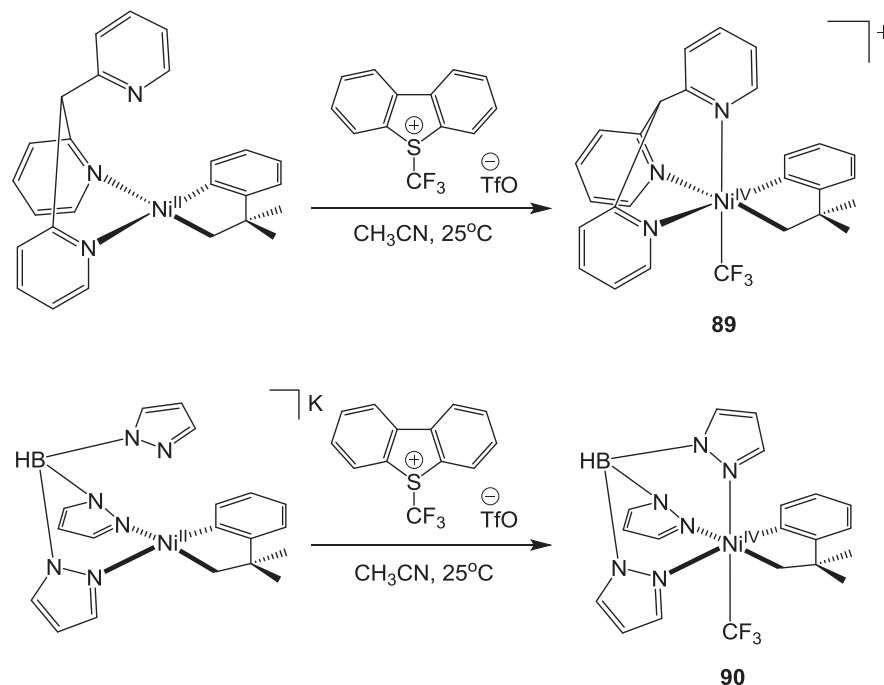


Fig. 44 Synthesis of complexes **89–90** two-electron oxidative trifluoromethylation.

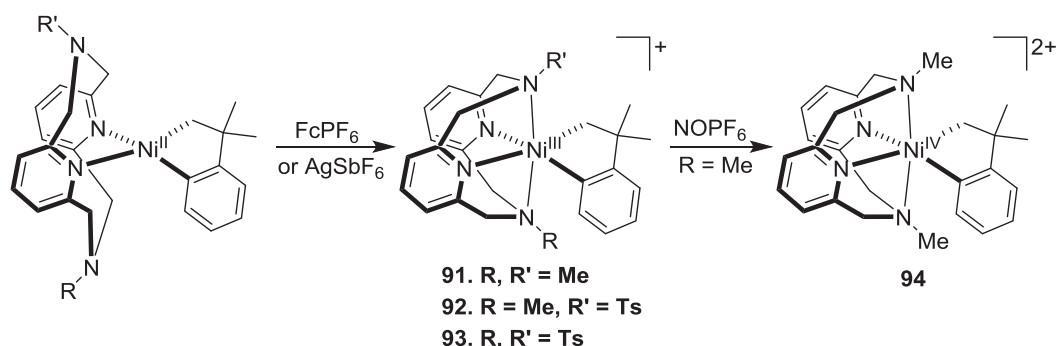


Fig. 45 Ni(III) complexes stabilized by ^RN4 and cycloneophyl ligands.

group is weakly coordinated to the metal center. However, in the EPR spectra of complex **93**, a rhombic signal with weak superhyperfine coupling to two axial nitrogens was observed, implying that both N_{Ts} groups bind weakly to the Ni metal center.

In 2017 the Mirica group demonstrated that cycloneophyl ligands could be used to stabilize high-valent Ni complexes when combined with a macrocyclic Me_3TACN (1,4,7-triazacyclononane) ligand. Oxidation of the Ni(II) precursor with FcPF_6 or FcBF_4 generated an uncommonly stable cationic Ni(III) complex **95**, which was characterized through X-ray crystallography and EPR spectroscopy (Fig. 46).⁷⁶ The complex adopted a square pyramidal geometry which was maintained in MeCN, as the EPR spectrum revealed a rhombic signal with superhyperfine coupling to only one N atom in the g_z direction, indicating a lack of an axially coordinated MeCN. Oxidation of **95** with $^{\text{Ac}}\text{FcBF}_4$ generated the first isolated dicationic Ni(IV) complex **96**, which adopted an octahedral geometry with an axially coordinated acetonitrile.

Utilizing a neutral tris(pyrazoyl)methane and an anionic tris(pyrazoyl)borate ligand along with a C-donor cycloneophyl ligand, Sanford et al. isolated a series of Ni(III) and Ni(IV) organometallic complexes **97–98** in 2019 (Fig. 47).⁷⁷ The Ni(III) complex **97-Py** was crystallized in pyridine to generate the octahedral complex with an axially coordinated pyridine ligand. EPR studies confirmed a Ni(III) metal center with $g_x = 2.23$, $g_y = 2.22$, and $g_z = 2.01$. Complex **98** was crystallized in MeCN, which generated an octahedral Ni(IV) complex with an axially coordinated MeCN ligand.

6.09.2.10 Ni Complexes With Miscellaneous Ligands

Cationic nickel imido complexes **99** and **100** were isolated by Hillhouse et al. in 2011, utilizing a 1,2-bis(di-*tert*-butylphosphino)ethane ligand. The neutral Ni(II) complexes were able to undergo a single electron oxidation to reach the cationic Ni(III) species (Fig. 48).⁷⁸ Notably, both adamantyl azide and 2,6-dimesitylphenylazide (dmp) were shown to be suitable for the formation of

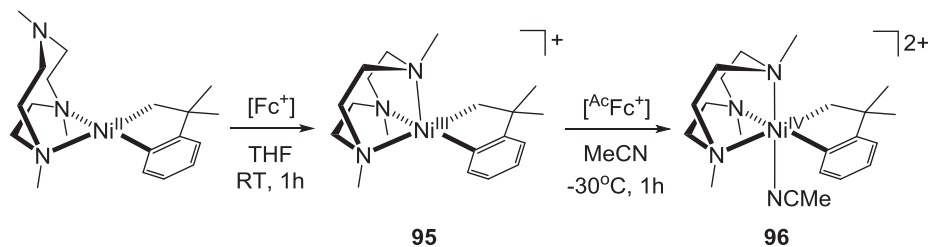


Fig. 46 Ni(III) and Ni(IV) complexes **95** and **96** stabilized by Me_3TACN and cycloneophyl ligands.

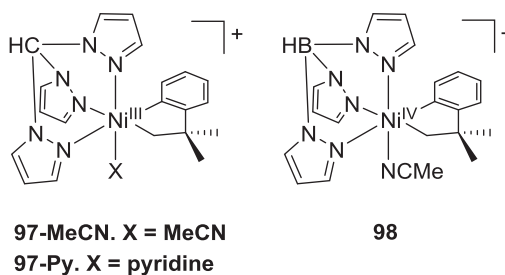


Fig. 47 Tris(pyrazol)methane and tris(pyrazol)borate Ni(III) and Ni(IV) Complexes **97–98**.

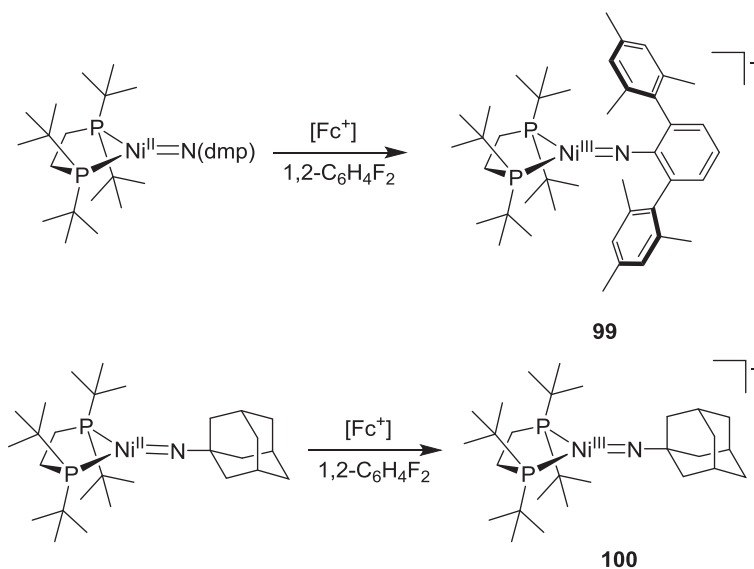
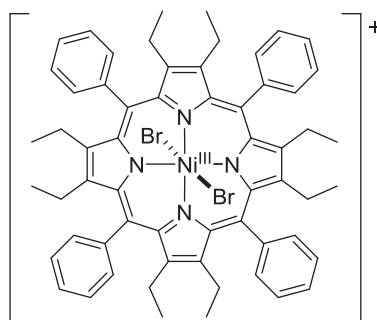


Fig. 48 Synthesis of Ni(III)-imide complexes **99** and **100** supported by bulky phosphine ligands.

Ni(III)-imido species. Both Ni(III)-imide complexes were analyzed using EPR spectroscopy and Evan's method to determine the magnetic moment. A temperature dependence in the magnetic moment was found for complex **99**, indicating that a high-spin/low-spin equilibrium is present. By comparing the magnetic moments of the two spin states with the expected values, a HS/LS ratio of approximately 1:4 was calculated at room temperature. EPR studies verified the presence of a low-spin d^7 Ni(III) center, with a single feature lacking superhyperfine coupling. The EPR spectrum of **100** shows a single feature, with the parameters $g_1 = 2.17$, $g_2 = 2.06$, and $g_3 = 1.97$. Notably, no spin equilibrium was observed in complex **100**.

In 2014, Chen et al. isolated a Ni(III) dihalide porphyrin complex **101** and were able to characterize the molecule through EPR and X-ray crystallography (Fig. 49).⁷⁹ An EPR spectrum obtained at 77 K revealed a ferromagnetically coupled signal with $g_x = 2.21$, $g_y = 2.10$, and $g_z = 2.13$. Variable temperature magnetic data revealing a magnetic moment of $\mu_b = 2.63$ with a $S = 1$, which the authors attributed to be either the Ni(III) high-spin state ($S = 3/2$) coupled to an antiparallel a_{2u} radical or the Ni(III) low-spin state ($S = 1/2$) interacting orthogonally with a parallel a_{1u} radical. Through DFT calculations and paramagnetic NMR analysis, the authors were able to confirm the triplet ground state of the complex was a low-spin Ni(III) metal center radical coupled to an a_{1u} porphyrin-based radical cation.



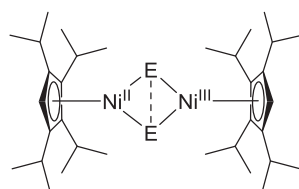
101

Fig. 49 The Ni(III)-dihalide porphyrin complex **101**.

In 2015, the Berry group analyzed a variety of diamagnetic chalcogen-bridged complexes $\text{Cp}_2^*\text{Ni}_2\text{E}_2$ ($\text{E} = \text{S}, \text{Se}, \text{Te}$) **102** and found that these complexes can be best electronically described as mixed-valent Ni(II)/(III) species (**Fig. 50**).⁸⁰ Three potential resonance forms were described based on the level of E-E interaction: a bimetallic Ni(II) species with an E-E single bond, a mixed Ni(II)/(III) species with an E-E $\frac{1}{2}$ order bond, and a bimetallic Ni(III) species with no E-E bonding. Through X-ray crystallography, Berry et al. were able to confirm that the E-E distances for these complexes was somewhere between a nonbonding interaction and a complete single bond, strengthening the assignment of the complexes as mixed Ni(II)/(III) species. Furthermore, reduction of **102-Se** drastically shortened the length of the Se-Se interaction compared to the neutral complex, consistent with the formation of a Se_2^{2-} species.

A variety of nickel bimetallic dithiolate complexes including three examples of Ni(III) complexes were isolated by Rauchfuss et al. in 2016 (**Fig. 51**).⁸¹ Varying the length of the alkyl chain of the dithiol backbone allowed for the isolation of several dinickel dithiolate complexes in varying geometries. A bimetallic Ni(III) propanedithiolate complex **103** was formed following the oxidation of the Ni(II) precursor with ferrocenium tetrafluoroborate. X-ray crystallography of **103** showed a 'butterfly' Ni_2S_2 core, while the Cp ligands adopted a cis geometry. A similar series of bimetallic complexes for the ethanedithiolate and diethanedithiol derivatives **104**–**105** were also synthesized and characterized through X-ray spectroscopy. Similar geometry changes were seen in the diethanedithiol complex, which adopted a geometry that allowed for metal-metal bonding following oxidation.

A unique trinuclear Rh_2Ni complex supported by N/S-type chelating ligands was synthesized by Konno et al. in 2017 that was shown to reversibly cycle between Ni(II), Ni(III), and Ni(IV) states (**Fig. 52**).⁸² The Ni(II) complex was shown to oxidize to Ni(III) in the presence of oxygen, and a reversible reduction pathway could be achieved with sodium borohydride. The Ni(III) species could subsequently be oxidized with cerium ammonium nitrate to generate the Ni(IV) complex which could be reduced back upon treatment with H_2O . Each of the complexes were characterized crystallographically, and a notable Jahn-Teller distortion was observed in the Ni(III) complex **107**, which was not present in complexes **106** or **108**. An EPR spectrum of complex **107** at 103 K showed an anisotropic signal with an average g value of 2.1, with no signal being detected for complexes **106** or **108**, further supporting the oxidation assignments. Furthermore, ^1H NMR spectroscopy performed on the d^6 $S = 0$ complex **108** provided validation for the Ni(IV) assignment.



102-S. E = S
102-Se. E = Se
102-Te. E = Te

Fig. 50 Chalcogen-bridged Ni_2E_2 complexes **102**.

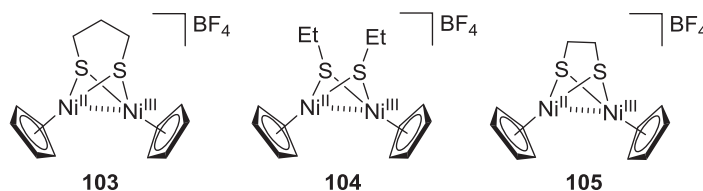


Fig. 51 Thiolate-supported dinuclear Ni(II)/Ni(III) complexes **103**–**105**.

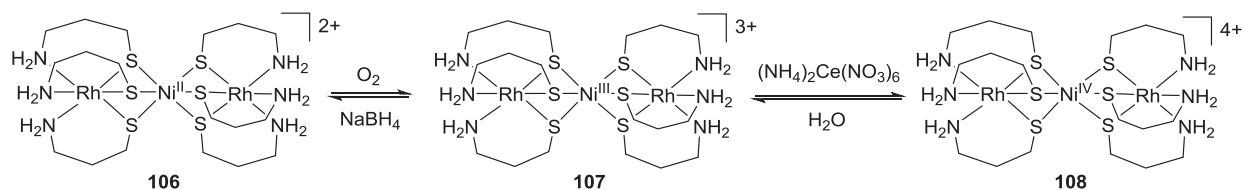


Fig. 52 The synthesis of RhNiRh trinuclear complexes **106–108**.

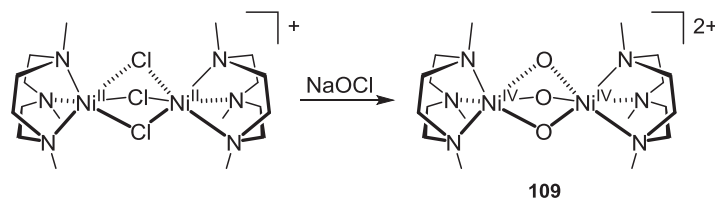


Fig. 53 Synthesis of dinuclear Ni^{IV} complex **109**.

Interestingly, in 2017 Browne et al. reported the oxidation with NaOCl of a dinuclear tris(μ -chloro)Ni(II) precursor supported by two 1,4,7-trimethyl-1,4,7-triazacyclononane ligands to generate the first dinuclear Ni(IV) complex **109** in which the two Ni(IV) centers are bridged by three μ -oxo groups (Fig. 53).⁸³ While this complex was not crystallographically characterized, detailed X-ray absorption spectroscopy (XAS), ESI-MS, resonance Raman, and computational studies provide support for the proposed structure for this Ni^{IV} species.

6.09.3 Summary and Outlook

Since the publication of the second edition of *Comprehensive Coordination Chemistry* in 2003, significant progress has been made by numerous research groups around the world in isolating high-valent Ni(III) and Ni(IV) complexes. A majority of this progress has been specific to the field of organometallic nickel chemistry, due largely to the increasing role that high-valent nickel species were shown to play in carbon-carbon and carbon-heteroatom bond forming reactions.

Within this chapter, we have attempted to thoroughly catalog both coordination and organometallic Ni(III) and Ni(IV) complexes that have been isolated since 2003. Furthermore, we have grouped complexes related to the general ligand frameworks used for their stabilization, along with providing brief synthetic routes to these high-valent complexes. Also discussed within this chapter are the key spectroscopic and physical characteristics of these complexes, which make them relevant for various research areas such as synthetic organometallic and bioinorganic chemistry.

We hope that a comprehensive grouping of such complexes along with the spectroscopic and physical characteristics provided will aid researchers in taking rational approaches toward the synthesis of a wider range of high-valent nickel species, as well as deciphering their roles in various oxidative transformations such as C–H bond activation and functionalization reactions.

References

- Tasker, S. Z.; Standley, E. A.; Jamison, T. F. *Nature* **2014**, *509*, 299–309.
- Boer, J. L.; Mulrooney, S. B.; Hausinger, R. P. *Arch. Biochem. Biophys.* **2014**, *544*, 142–152.
- Zheng, B.; Tang, F.; Luo, J.; Schultz, J. W.; Rath, N. P.; Mirica, L. M. *J. Am. Chem. Soc.* **2014**, *136*, 6499–6504.
- Camasso, N. M.; Sanford, M. S. *Science* **2015**, *347*, 1218–1220.
- Organometallic Chemistry of High-Valent Ni(III) and Ni(IV) Complexes. In *Nickel Catalysis in Organic Synthesis*; Mirica, L. M., Smith, S. M., Griego, L., Ogoshi, S., Eds., Wiley-VCH, 2019; pp 223–248.
- King, R. B. *Encyclopedia of Inorganic Chemistry*, 2nd ed.; John Wiley and Sons, Inc., 2006.
- Kubiak, C. P.; Simón-Manso, E.; Cámpora, J.; Zargarian, D. *Comprehensive Organometallic Chemistry III*; Elsevier Science, 2007.
- Carnes, M.; Buccella, D.; Chen, J. Y. C.; Ramirez, A. P.; Turro, N. J.; Nuckolls, C.; Steigerwald, M. *Angew. Chem., Int. Ed.* **2009**, *48*, 290–294.
- Nomura, M.; Geoffroy, M.; Adkine, P.; Fourmigué, M. *Eur. J. Inorg. Chem.* **2006**, *2006*, 5012–5021.
- Nomura, M.; Cauchy, T.; Fourmigué, M. *Coord. Chem. Rev.* **2010**, *254*, 1406–1418.
- Duan, H.-B.; Ren, X.-M.; Meng, Q.-J. *Coord. Chem. Rev.* **2010**, *254*, 1509–1522.
- Garreau-de Bonneval, B.; Moineau-Chane Ching, K. I.; Alary, F.; Bui, T.-T.; Valade, L. *Coord. Chem. Rev.* **2010**, *254*, 1457–1467.
- Deplano, P.; Pillá, L.; Espa, D.; Mercuri, M. L.; Serpe, A. *Coord. Chem. Rev.* **2010**, *254*, 1434–1447.
- Kishida, H.; Matsuzaki, H.; Okamoto, H.; Manabe, T.; Yamashita, M.; Taguchi, Y.; Tokura, Y. *Nature* **2000**, *405*, 929–932.
- Wu, H.; Kawakami, D.; Sasaki, M.; Xie, J.; Takaishi, S.; Kajiwara, T.; Miyasaka, H.; Yamashita, M.; Matsuzaki, H.; Okamoto, H. *Inorg. Chem.* **2007**, *46*, 7410–7413.
- Mitsumi, M.; Yoshida, Y.; Kohyama, A.; Kitagawa, Y.; Ozawa, Y.; Kobayashi, M.; Toriumi, K.; Tadokoro, M.; Ikeda, N.; Okumura, M.; Kurmoo, M. *Inorg. Chem.* **2009**, *48*, 6680–6691.
- Hashiguchi, R.; Otsubo, K.; Maesato, M.; Sugimoto, K.; Fujiwara, A.; Kitagawa, H. *Angew. Chem., Int. Ed.* **2017**, *56*, 3838–3841.

18. Kogut, E.; Wiencko, H. L.; Zhang, L. B.; Cordeau, D. E.; Warren, T. H. *J. Am. Chem. Soc.* **2005**, *127*, 11248–11249.
19. Cho, J.; Furutachi, H.; Fujinami, S.; Toshi, T.; Ohtsu, H.; Ikeda, O.; Suzuki, A.; Nomura, A.; Uruga, T.; Tanida, H.; Kawai, T.; Tanaka, K.; Kitagawa, T.; Suzuki, M. *Inorg. Chem.* **2006**, *45*, 2873–2885.
20. Morimoto, Y.; Takagi, Y.; Saito, T.; Ohta, T.; Ogura, T.; Tohnai, N.; Nakano, M.; Itoh, S. *Angew. Chem., Int. Ed.* **2018**, *57*, 7640–7643.
21. Cho, J.; Sarangi, R.; Annaraj, J.; Kim, S. Y.; Kubo, M.; Ogura, T.; Solomon, E. I.; Nam, W. *Nat. Chem.* **2009**, *1*, 568–572.
22. Cho, J.; Kang, H. Y.; Liu, L. V.; Sarangi, R.; Solomon, E. I.; Nam, W. *Chem. Sci.* **2013**, *4*, 1502–1508.
23. Kim, J.; Shin, B.; Kim, H.; Lee, J.; Kang, J.; Yanagisawa, S.; Ogura, T.; Masuda, H.; Ozawa, T.; Cho, J. *Inorg. Chem.* **2015**, *54*, 6176–6183.
24. Nishigaki, J.-I.; Matsumoto, T.; Tatsumi, K. *Inorg. Chem.* **2012**, *51*, 3690–3697.
25. Bhowmick, I.; Roehl, A. J.; Neilson, J. R.; Rappe, A. K.; Shores, M. P. *Chem. Sci.* **2018**, *9*, 6564–6571.
26. Lipschutz, M. I.; Yang, X.; Chatterjee, R.; Tilley, T. D. *J. Am. Chem. Soc.* **2013**, *135*, 15298.
27. Schultz, J. W.; Fuchigami, K.; Zheng, B.; Rath, N. P.; Mirica, L. M. *J. Am. Chem. Soc.* **2016**, *138*, 12928–12934.
28. Smith, S. M.; Rath, N. P.; Mirica, L. M. *Organometallics* **2019**, *38*, 3602–3609.
29. Berry, J. F.; Bothe, E.; Cotton, F. A.; Ibragimov, S. A.; Murillo, C. A.; Villagran, D.; Wang, X. P. *Inorg. Chem.* **2006**, *45*, 4396–4406.
30. Diccianni, J. B.; Hu, C. H.; Diao, T. N. *Angew. Chem., Int. Ed.* **2016**, *55*, 7534–7538.
31. Alonso, P. J.; Arauzo, A. B.; García-Monforte, M. A.; Martín, A.; Menjón, B.; Rillo, C.; Tomás, M. *Chem. – Eur. J.* **2009**, *15*, 11020–11030.
32. Zhao, N.; Filatov, A. S.; Xie, J.; Hill, E. A.; Anderson, J. S. *J. Am. Chem. Soc.* **2020**, *142*, 21634–21639.
33. Cao, T.-P.-A.; Nocton, G.; Ricard, L.; Le Goff, X. F.; Auffrant, A. *Angew. Chem., Int. Ed.* **2014**, *53*, 1368–1372.
34. Ay, B.; Gönül, İ.; Demir, B. S.; Saygıdeğer, Y.; Kani, İ. *Inorg. Chem. Commun.* **2020**, *114*, 107824.
35. Diccianni, J. B.; Hu, C. H.; Diao, T. N. *Angew. Chem., Int. Ed.* **2017**, *56*, 3635–3639.
36. Fisher, K. J.; Feuer, N. L.; Lant, H. M. C.; Mercado, B. Q.; Crabtree, R. H.; Brudvig, G. W. *Chem. Sci.* **2020**, *11*, 1683–1690.
37. van Gastel, M.; Shaw, J. L.; Blake, A. J.; Flores, M.; Schroder, M.; McMaster, J.; Lubitz, W. *Inorg. Chem.* **2008**, *47*, 11688–11697.
38. Stephen, E.; Huang, D.; Shaw, J. L.; Blake, A. J.; Collison, D.; Davies, E. S.; Edge, R.; Howard, J. A. K.; McInnes, E. J. L.; Wilson, C.; Wolowska, J.; McMaster, J.; Schröder, M. *Chem. – Eur. J.* **2011**, *17*, 10246–10258.
39. Chen, C.-H.; Lee, G.-H.; Liaw, W.-F. *Inorg. Chem.* **2006**, *45*, 2307–2316.
40. Lee, C. M.; Chuang, Y. L.; Chiang, C. Y.; Lee, G. H.; Liaw, W. F. *Inorg. Chem.* **2006**, *45*, 10895–10904.
41. Chiou, T. W.; Liaw, W. F. *Inorg. Chem.* **2008**, *47*, 7908–7913.
42. Lee, C. M.; Chen, C. H.; Liao, F. X.; Hu, C. H.; Lee, G. H. *J. Am. Chem. Soc.* **2010**, *132*, 9256–9258.
43. Lai, K.-T.; Ho, W.-C.; Chiou, T.-W.; Liaw, W.-F. *Inorg. Chem.* **2013**, *52*, 4151–4153.
44. Chiou, T.-W.; Tseng, Y.-M.; Lu, T.-T.; Weng, T.-C.; Sokaras, D.; Ho, W.-C.; Kuo, T.-S.; Jang, L.-Y.; Lee, J.-F.; Liaw, W.-F. *Chem. Sci.* **2016**, *7*, 3640–3644.
45. Lee, C. M.; Chiou, T. W.; Chen, H. H.; Chiang, C. Y.; Kuo, T. S.; Liaw, W. F. *Inorg. Chem.* **2007**, *46*, 8913–8923.
46. Chang, H. C.; Lin, S. H.; Hsu, Y. C.; Jen, S. W.; Lee, W. Z. *Dalton Trans.* **2018**, *47*, 3796–3802.
47. Gu, N. X.; Oyala, P. H.; Peters, J. C. *J. Am. Chem. Soc.* **2020**, *142*, 7827–7835.
48. Kuwamura, N.; Kitano, K.; Hirotsu, M.; Nishioka, T.; Teki, Y.; Santo, R.; Ichimura, A.; Hashimoto, H.; Wright, L. J.; Kinoshita, I. *Chem. – Eur. J.* **2011**, *17*, 10708–10715.
49. Zhou, W.; Schultz, J. W.; Rath, N. P.; Mirica, L. M. *J. Am. Chem. Soc.* **2015**, *137*, 7604–7607.
50. Zhou, W.; Rath, N. P.; Mirica, L. M. *Dalton Trans.* **2016**, *45*, 8693–8695.
51. Zhou, W.; Zheng, S. A.; Schultz, J. W.; Rath, N. P.; Mirica, L. M. *J. Am. Chem. Soc.* **2016**, *138*, 5777–5780.
52. Zhou, W.; Watson, M. B.; Zheng, S.; Rath, N. P.; Mirica, L. M. *Dalton Trans.* **2016**, *137*, 15886–15893.
53. Lee, H.; Borgel, J.; Ritter, T. *Angew. Chem., Int. Ed.* **2017**, *56*, 6966–6969.
54. Roy, P.; Bour, J. R.; Kampf, J. W.; Sanford, M. S. *J. Am. Chem. Soc.* **2019**, *141*, 17382–17387.
55. Zhang, S. K.; Struwe, J.; Hu, L.; Ackermann, L. *Angew. Chem., Int. Ed.* **2020**, *59*, 3178–3183.
56. Meucci, E. A.; Camasso, N. M.; Sanford, M. S. *Organometallics* **2017**, *36*, 247–250.
57. Meucci, E. A.; Ariafard, A.; Canty, A. J.; Kampf, J. W.; Sanford, M. S. *J. Am. Chem. Soc.* **2019**, *141*, 13261–13267.
58. Pandarus, V.; Zargarian, D. *Organometallics* **2007**, *26*, 4321–4334.
59. Spasyuk, D. M.; Zargarian, D.; van der Est, A. *Organometallics* **2009**, *28*, 6531–6540.
60. Mougang-Soume, B.; Belanger-Gariepy, F.; Zargarian, D. *Organometallics* **2014**, *33*, 5990–6002.
61. Mousa, A. H.; Bendix, J.; Wendt, O. F. *Organometallics* **2018**, *37*, 2581–2593.
62. Kozhanov, K. A.; Bubnov, M. P.; Cherkasov, V. K.; Fukin, G. K.; Vavilina, N. N.; Efreмова, L. Y.; Abakumov, G. A. *J. Mag. Res.* **2009**, *197*, 36–39.
63. Cloutier, J. P.; Rechinat, L.; Canac, Y.; Ess, D. H.; Zargarian, D. *Inorg. Chem.* **2019**, *58*, 3861–3874.
64. Martinez, G. E.; Ocampo, C.; Park, Y. J.; Fout, A. R. *J. Am. Chem. Soc.* **2016**, *138*, 4290–4293.
65. Yu, S.; Dudkina, Y.; Wang, H.; Kholin, K. V.; Kadirov, M. K.; Budnikova, Y. H.; Vicić, D. A. *Dalton Trans.* **2015**, *44*, 19443–19446.
66. Kosobokov, M. D.; Sandleben, A.; Vogt, N.; Klein, A.; Vicić, D. A. *Organometallics* **2018**, *37*, 1086.
67. Tang, F. Z.; Rath, N. P.; Mirica, L. M. *Chem. Comm.* **2015**, *51*, 3113–3116.
68. Bour, J. R.; Camasso, N. M.; Sanford, M. S. *J. Am. Chem. Soc.* **2015**, *137*, 8034–8037.
69. Chong, E.; Kampf, J. W.; Ariafard, A.; Canty, A. J.; Sanford, M. S. *J. Am. Chem. Soc.* **2017**, *139*, 6058–6061.
70. D'Accrisio, F.; Borja, P.; Saffon-Merceron, N.; Fustier-Boutignon, M.; Mezailes, N.; Nebra, N. *Angew. Chem., Int. Ed.* **2017**, *56*, 12898–12902.
71. Roberts, C. C.; Chong, E.; Kampf, J. W.; Canty, A. J.; Ariafard, A.; Sanford, M. S. *J. Am. Chem. Soc.* **2019**, *141*, 19513–19520.
72. Bour, J. R.; Ferguson, D. M.; McClain, E. J.; Kampf, J. W.; Sanford, M. S. *J. Am. Chem. Soc.* **2019**, *141*, 8914–8920.
73. Meucci, E. A.; Nguyen, S. N.; Camasso, N. M.; Chong, E.; Ariafard, A.; Canty, A. J.; Sanford, M. S. *J. Am. Chem. Soc.* **2019**, *141*, 12872–12879.
74. Shreiber, S. T.; DiMucci, I. M.; Khrižanforov, M. N.; Titus, C. J.; Nordlund, D.; Dudkina, Y.; Cramer, R. E.; Budnikova, Y.; Lancaster, K. M.; Vicić, D. A. *Inorg. Chem.* **2020**, *59*, 9143–9151.
75. Smith, S. M.; Planas, O.; Gomez, L.; Rath, N.; Ribas, X.; Mirica, L. M. *Chem. Sci.* **2019**, *10*, 10366–10372.
76. Watson, M. B.; Rath, N. P.; Mirica, L. M. *J. Am. Chem. Soc.* **2017**, *139*, 35–38.
77. Roberts, C. C.; Camasso, N. M.; Bowes, E. G.; Sanford, M. S. *Angew. Chem., Int. Ed.* **2019**, *58*, 9104–9108.
78. Iluc, V. M.; Miller, A. J. M.; Anderson, J. S.; Monreal, M. J.; Mehn, M. P.; Hillhouse, G. L. *J. Am. Chem. Soc.* **2011**, *133*, 13055–13063.
79. Cheng, R.-J.; Ting, C.-H.; Chao, T.-C.; Tseng, T.-H.; Chen, P. Y. *Chem. Comm.* **2014**, *50*, 14265–14268.
80. Yao, S. A.; Martin-Diaconescu, V.; Infante, I.; Lancaster, K. M.; Gotz, A. W.; DeBeer, S.; Berry, J. F. *J. Am. Chem. Soc.* **2015**, *137*, 4993–5011.
81. Chambers, G. M.; Rauchfuss, T. B.; Arrigoni, F.; Zampella, G. *Organometallics* **2016**, *35*, 836–846.
82. Kouno, M.; Yoshinari, N.; Kuwamura, N.; Yamagami, K.; Sekiyama, A.; Okumura, M.; Konno, T. *Angew. Chem., Int. Ed.* **2017**, *56*, 13762–13766.
83. Padamati, S. K.; Anielone, D.; Draksharapu, A.; Primi, G.; Martin, D. J.; Tromp, M.; Swart, M.; Browne, W. R. *J. Am. Chem. Soc.* **2017**, *139*, 8718–8724.